

**High precision spectroscopy of Λ hypernuclei
with the (π^+, K^+) reaction
at the High Intensity High Resolution beamline**

HIHR Hypernuclear Collaboration

Satoshi N. Nakamura^{*,1}, Takeru Akiyama¹, Rogers Anya¹, Hiroyuki Fujioka²
Tomomasa Fujiwara¹, Toshiyuki Gogami³, Shuhei H. Hayakawa¹,
Ryotaro Honda⁴, Yuji Ishikawa¹, Kosuke Itabashi¹, Shunsuke Kajikawa¹,
Kento Kamada¹, Honoka Kanauchi¹, Masashi Kaneta¹, Ryoko Kino¹,
Tomomasa Kitaoka¹, Takeshi Koike¹, Koji Miwa¹, Masaya Mizuno¹,
Pete Markowitz⁵, Taito Morino¹, Tomofumi Nagae³, Shintaro Nagano¹,
Sho Nagao¹, Yuki R. Nakamura¹, Hiroyuki Noumi⁶, Kazuki Okuyama¹,
Fumiya Oura¹, Tamao Sakao¹, Fuminori Sakuma⁷, Kotaro Shirotori⁶,
Koga Tachibana¹, Hitoshi Takahashi⁴, Toshiyuki Takahashi⁴,
Hirokazu Tamura¹, Yuichi Toyama¹, Keita Uehara¹, Mifuyu Ukai^{4,1},
Shunsuke Wada¹, Junya Yoshida¹

¹*Department of Physics, Graduate School of Science, Tohoku University*

²*School of Science, Tokyo Institute of Technology*

³*Graduate School of Science, Kyoto University*

⁴*Institute of Particle and Nuclear Studies, KEK*

⁵*Florida International University*

⁶*Research Center for Nuclear Physics, Osaka University*

⁷*RIKEN*

*Contact and Spokesperson: nue@tohoku.ac.jp

Abstract

The recent observation of neutron stars with masses accurately measured to be larger than two solar masses posed a challenge to our present knowledge of the interaction among baryons in high-density matter. In the interior of a neutron star which is highly asymmetric nuclear matter, nucleons reach densities overcoming the one of nuclei by several times. In these conditions, the appearance of strangeness, in the form of hyperons, is energetically favored since it helps to reduce the Fermi energy of nucleons. However, present theoretical models typically predict that this energy reduction (and the consequent "softening" of the Equation of State) would lead to neutron stars with a mass smaller than $1.5M_{\odot}$. This is the so-called "hyperon puzzle", that is currently one of the unsolved key issues in the physics of compact stars.

There is a consensus that there are any mechanisms to harden neutron stars or to suppress appearance of hyperons, therefore baryonic interaction at high density should be more repulsive than what supposed so far, and hypernuclear spectroscopy data are necessary to constrain it.

Relating the experimental findings on hypernuclei to the equation of state of dense matter is a highly non-trivial task. The key issue is an accurate determination of the hyperon-nucleon interaction.

There are growing efforts worldwide in hypernuclear spectroscopy: needless to say, J-PARC is the center of hypernuclear spectroscopic study; JLab has a campaign of hypernuclear physics programs to investigate iso-spin and mass dependence of Λ hypernuclei with electron beams; the decay-pion spectroscopy of hyperhydrogen has achieved great success at Mainz and a study of hypernuclei with heavy ion beams was started at GSI.

The (π^+, K^+) reaction spectroscopy played a key role in investigation of $S = -1$ hypernuclei studies and the J-PARC MR synchrotron can provide world's strongest π^+ beam with an energy enough to produce strangeness. However, the energy resolution of the (π^+, K^+) reaction spectroscopy has been limited to a few MeV due to quality of secondary produced π^+ beams and intensity of the beam has been limited by the beamline detectors.

An ambitious and challenging experimental program was started at J-PARC, the extension of the hadron experimental hall. The High Intensity High Resolution beamline (HIHR) is one of major facilities of the project. HIHR enables us to remove the limitation of acceptable π^+ beam intensity and maximize potential of the MR synchrotron.

The proposed experiment explores wide mass range of Lambda hypernuclei with unprecedented energy resolution at the HIHR beamline to solve the hyperon puzzle.

Contents

| | |
|--|----|
| 1. Introduction | 4 |
| 2. Proposed experiment | 7 |
| 2.1 Neutron stars and the hyperon puzzle | 13 |
| 2.2 Theoretical models of structure calculation of Λ hypernuclei | 18 |
| 2.3 Choice of targets, additional physics outputs | 25 |
| 2.4 International competition and collaboration | 28 |
| 3. Experimental setup | 30 |
| 3.1 High Intensity High Resolution beamline | 30 |
| 3.2 Kinematics and key parameters of HIHR beamline and spectrometer | 32 |
| 3.3 Beamline and K spectrometer dispersion match setting | 35 |
| 3.4 Detectors for the kaon spectrometer | 38 |
| 4. Yield estimation | 40 |
| 4.1 Primary target and π^+ beam extraction | 40 |
| 4.2 Solid angle estimation of the kaon spectrometer | 44 |
| 4.3 Yield estimation of ${}^{12}_{\Lambda}\text{C}$ | 46 |
| 5. Resolution estimation | 47 |
| 5.1 TRANSPORT, optics code study | 47 |
| 5.2 GEANT4, Monte Carlo simulation study | 51 |
| 5.3 Summary of energy resolution study | 55 |
| 6. Beamtime request | 57 |
| 7. Summary | 61 |

1. Introduction

The major goal of nuclear physics is understanding the nature of many-body system whose dynamics is dictated by the strong interaction. There is a hierarchy of three such systems in our universe: 1) baryons/mesons, the bound system of quarks, 2) nuclei, the self-bound system of baryons and 3) neutron stars, isospin-asymmetric nuclear matter bound by the gravitational force. The size scale of 1) and 2) is femtometers and that of 3) is ~ 10 km. Though they differ by 10^{19} order of magnitudes, it is common that the strong interaction plays a key role to govern their structure and properties. The strong interaction in the low energy region where the QCD is not perturbative has been investigated in the framework of baryon potential models. The construction of NN potentials has taken advantage upon the availability of a substantial number of scattering data. High-precision potential models fit all these data with extreme accuracy. However, when only two-body forces are accounted for, light nuclei turn out to be under-bound and the saturation properties of infinite isospin-symmetric nuclear matter are not correctly reproduced. It indicates the need for a three-body interaction. The same theoretical framework could be extended to the strange sector. Though the strange quark is heavier than the u and d quarks, it is still lighter than the QCD cut-off (~ 1 GeV) unlike the heavy quarks (c , t , b). Hence, the strange quark can be treated in the framework of the flavor SU(3) symmetry which is a natural extension of the isospin symmetry for ordinary nucleons. To devise a unified description of the baryonic interaction within the flavor SU(3) basis, one must then quantitatively understand the hyperon-nucleon (YN) and the hyperon-hyperon (YY) interactions. Investigation on double- Λ and Ξ , $S = -2$ hypernuclei and direct measurement of YN scattering experiments made great progresses at the existing J-PARC hadron hall. However, the bare YN interaction and effective YN interaction in nuclei are different due to quantum many-body effects; spectroscopic investigation of Λ -hypernuclei, nuclear many-body systems containing one Λ particle, provides a unique and, currently, the only practical tool to provide effective YN interaction in various nuclei with an excellent precision.

While several models of YN forces were proposed in the past, recent observation of neutron stars with masses of $2M_{\odot}$ (two solar mass) poses several important questions. There is a very simple argument to justify the appearance of strange degrees of freedom in the inner core of

a neutron star. In the pure neutron matter case, whenever the chemical potential becomes sufficiently large to match the chemical potential of a hyperon in the same matter, the hyperon becomes stable since it is a distinguishable particle, and creates its own Fermi sea, thereby lowering the kinetic energy of the system. This results in a so-called "softening" of the equation of state (EOS), due to a decrease of the Fermi pressure. In turn, a soft EOS predicts a lower sustainable mass for a neutron star. So far, existing YN interactions typically predict a maximum mass no larger than $1.5M_{\odot}$, in strong contrast with the astrophysical observations (the "hyperon puzzle"). The key for solving this apparent contradiction is a more repulsive YN interaction, which increases the hyperon chemical potential, moving the onset of hyperons at higher densities. Most models nowadays agree on this aspect, but additional constraints are needed, and they can only be inferred from accurate spectroscopic data of hypernuclei.

The relation between hypernuclei and matter inside a neutron star is not straightforward. It is clear that the hyperon chemical potential at high density cannot be effectively constrained from the existing hypernuclear data with a few MeV resolution, unless very accurate measurements on hypernuclei are performed in wide mass range. Tiny changes in the binding energy, and consequently on the determination of the YN/YNN force, can have dramatic consequences on the EOS of matter at supra-saturation conditions.

Another interesting aspect of the YN interaction is the charge symmetry breaking (CSB). Recently decay-pion spectroscopy of electro-produced ${}^4_{\Lambda}\text{H}$, which was originally proposed at JLab [LER13], was successfully carried out at Mainz [ESS15] and the excitation energy of ${}^4_{\Lambda}\text{He}$ 1^+ state was also successfully measured by the gamma-spectroscopy at J-PARC [TOY15]. These new experimental data strongly support the fact that the $A=4$ hypernuclear isospin-doublet has a large CSB for the ground states (0^+) and small CSB for the 1^+ excited states. Although the origin of such a large CSB is not fully understood, it is clear that the discussion based on two-body YN/NN interaction only does not suffice and that the inclusion of $\Lambda\text{N}-\Sigma\text{N}$ coupling and three-body force are essential. For heavier and neutron richer hypernuclear systems, such $\Lambda\text{N}-\Sigma\text{N}$ coupling and 3-body force become more important, implying that the behavior of Λ in symmetric nuclear matter and neutron-rich environments would be quite different.

Though a systematic study of $A \leq 208$ Λ hypernuclei with a few MeV accuracy has already been carried out with the conventional (π^+, K^+) reaction spectroscopy at BNL-AGS and KEK-PS [PIL91,HAS95,HAS96,HAS98,HOT01], the accuracy of existing hypernuclear data is not adequate to the features of the baryonic force models needed to properly address the hyperon puzzle, and thus higher precision data are necessary.

We propose to measure Λ binding energies of Λ hypernuclei in wide mass region via the (π^+, K^+) reaction at the HIHR beamline which will be realized in the extended hadron experimental hall of J-PARC. **Precise hypernuclear spectroscopy in wide mass region is crucially important to constrain or provide necessary information to construct a reliable interaction which can be used to calculate EOS of the neutron stars. Such high precision hypernuclear spectroscopy is only possible at momentum dispersion match π beamline, HIHR and cannot be performed at other facilities.**

2. Proposed experiment

The proposed experiment investigates Λ hypernuclei in wide mass range with the ${}^A Z(\pi^+, K^+) {}^A_\Lambda Z$ reaction (Fig. 2-1).



Figure 2-1: The elementary process of the $n(\pi^+, K^+) \Lambda$. A neutron in a nucleus is converted by this reaction to a Λ hyperon. Some fraction of produced Λ is stuck to the nucleus to produce a Λ hypernucleus.

There are various methods for hypernuclear spectroscopy. It can be categorized in the reaction spectroscopy such as the missing mass spectroscopy with the (π^+, K^+) reaction and others which include decay product studies such as gamma and decay-pion spectroscopies. The production information is complementary to the information obtained by decay product studies.

Reaction spectroscopy with the missing mass technique is quite powerful way of investigation of hypernuclei. It provides reaction cross sections and detailed information of energy levels of hypernuclear states.

The hypernuclear reaction spectroscopy started with the (K^-, π^-) reaction. An s -quark in the beam K^- is exchanged with a d -quark in a neutron to produce a Λ in the (K^-, π^-) reaction. On the other hand, the (π^+, K^+) reaction produces s and \bar{s} quark pair associatively and the a Λ and a K^+ are produced simultaneously. These reactions convert a neutron to a Λ , and thus both (K^-, π^-) and (π^+, K^+) reactions produced the same hypernuclei with the same targets while they are exothermic and endothermic reactions.

Typical cross sections of Λ hypernuclei for these reactions are 1 mb/sr and 10 μ b/sr for (K^-, π^-) and (π^+, K^+) reactions, respectively.

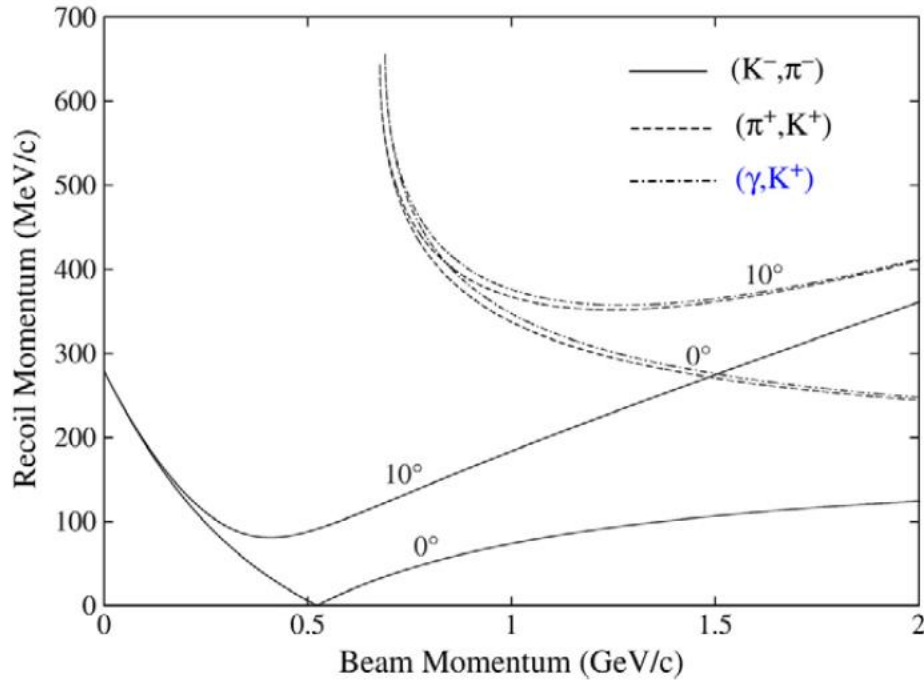


Figure 2-2: Beam momentum dependence of hypernuclear recoil momentum with a ^{12}C target for various reactions [HAS06].

Figure 2-2 shows recoil momentum transfer to the produced hypernuclei as a function of beam momentum. The (K^-, π^-) reaction gives small momentum transfer, and thus a neutron is converted to a Λ without changing angular momentum. It populates predominantly substitutional states; the produced Λ occupies the orbit with the same angular momentum as the converted neutron. Contrary to the (K^-, π^-) reaction, (π^+, K^+) and $(\gamma, K^+) / (e, e'K^+)$ give large momentum transfer to hypernuclei and they can populate high-spin states with a neutron hole in large angular momentum orbits and a Λ in small angular momentum states. This feature allows (π^+, K^+) reaction to have a large cross section to populate deeply bound Λ states like a ground state by converting a neutron with a high angular momentum to a Λ in s orbit while the cross section of such a state is highly suppressed for the (K^-, π^-) reaction due to small angular momentum transfer.

The $(e, e'K^+)$ reaction has similar features to populate deep bound Λ hypernuclei as the (π^+, K^+) reaction, because both are endothermic reactions and momentum transfer is large. However, its hypernuclear production cross section is extremely small, $0.1 \mu\text{b}/\text{sr}$ which is 100 times less than it of the (π^+, K^+) reaction. In order to compensate small production cross section, very high intensity primary electron beam ($100 \mu\text{A} = 6.3 \times 10^{14} e^-/\text{sec}$) is

used. High quality electron beam allows to avoid measuring momentum and position of electron beams and combination of high-resolution spectrometers for kaon and scattered electrons make it possible to measure hypernuclear mass with a resolution of 0.5 MeV (FWHM) , however accidental coincidence background originating from the high intensity primary electron beam causes a serious problem about signal-to-noise ratio [TAN14, GOG18].

So far, the (π^+, K^+) reaction spectroscopy has limitations for resolution as well as hypernuclear yields. Since π^+ beam is produced as the secondary particles and its large momentum spread makes analysis of beam momentum inevitable. Intensity of π^+ beam is limited by operational rate limit of detector system on the beamline. Due to these reasons, the energy resolution and beam intensity for the (π^+, K^+) hypernuclear spectroscopy have been limited to be a few MeV and several million π^+ s per a second, respectively.

Introduction of HIHR will remove those limitations from the (π^+, K^+) Λ hypernuclear spectroscopy and it will realize the energy resolution of 0.4 MeV (FWHM) which is equivalent or better than it of $(e, e'K^+)$ spectroscopy and such a good energy resolution enables us to determine binding energies of various Λ hypernuclei with an accuracy of <100 keV. Furthermore, there is no limitation for π^+ beam intensity. Detail of HIHR will be given in section 3.

It should be noted that the (π^+, K^+) reaction populates spin non-flip states in forward angles while the $(\gamma, K^+) / (e, e'K^+)$ reaction populates both spin-flip and non-flip states because photon has spin 1. This spin states selectivity of the (π^+, K^+) reaction spectroscopy may simplify the analysis of heavy hypernuclei of which density of energy levels becomes high. Since the (π^+, K^+) reaction converts a neutron to a Λ and the $(e, e'K^+)$ reaction converts a proton, different hypernuclei which belong to the same iso-spin multiplet will be studied with the same target. They are highly complementary, and it is important to have the same level of accuracy for these reaction spectroscopic techniques in order to discuss subtle effect of charge symmetry breaking effects of the ΛN interaction.

Table 2-I summarizes the features of (K^-, π^-) , (π^+, K^+) and $(e, e'K^+)$ reaction spectroscopy of Λ hypernuclei.

After the first proposal of the (π^+, K^+) reaction spectroscopy by H.Thiessem [THI80], pioneering experiments were performed at BNL AGS [MIL85, PIL91] and then intensive research was carried out at KEK-PS with SKS spectrometer [HAS95, HAS96, HAS98, HOT01].

Table 2-I: Reactions for Λ hypernuclear spectroscopy

| Reaction | Resolution (MeV, FWHM) | Cross section ($\mu\text{b/sr}$) for light targets | Momentum Transfer | Elementary process | Signal to Noise ratio |
|----------------|--|--|-------------------|------------------------|-----------------------|
| (K^-, π^-) | >2 | 1000 | Small | $n(K^-, \pi^-)\Lambda$ | \bigcirc |
| (π^+, K^+) | 1.5 \rightarrow 0.4 (HIHR) | 10 | Large | $n(\pi^+, K^+)\Lambda$ | \bigcirc |
| $(e, e'K^+)$ | 0.5 | 0.1 | Large | $p(e, e'K^+)\Lambda$ | \times |

Figure 2-3 shows Λ binding energy spectra of $^{12}_{\Lambda}\text{C}$ measured with the (π^+, K^+) reaction at BNL-AGS, KEK-SKS and J-PARC-HIHR (expectation). The energy resolutions are respectively 3 MeV, 1.5 MeV and 0.4 MeV (expectation) for BNL, KEK and HIHR. Comparing the spectra from BNL and KEK, one can easily see that a factor of two improvement of the energy resolution provides much richer information. Further improvement of energy resolution from KEK to HIHR by a factor of more than three, determination precision of energies for major peaks which correspond to Λ in s, p -orbits is improved drastically as well as it will enable us to separate sub-peaks originating from core nucleus excited states. Since heavier hypernuclei have more complex nuclear structure, better energy resolution contributes to improve sensitivity of small cross section peaks.

Figure 2-4 shows $^{208}_{\Lambda}\text{Pb}$ energy spectrum measured with SKS at KEK [HAS96] and peaks corresponding to the states with Λ in s, p, d, f, g, h -orbits are barely observed for a major neutron hole series of $(i_{13/2})^{-1}$ but a clear observation of these peaks was hampered by overlapping with sub-major neutron series from a neutron hole in $(h_{9/2})^{-1}$ where a neutron was converted to a Λ . Due to small cross section of $^{208}_{\Lambda}\text{Pb}$, a thicker target (3.418 g/cm^2) was used at SKS and it results in energy resolution of 2.3 MeV (FWHM), though a thinner carbon target (0.859 g/cm^2) was used to achieve so far best energy resolution of 1.45 MeV as the (π^+, K^+) reaction. Sub-MeV resolution is necessary to observe clear peaks for heavy hypernuclei and a high intensity π^+ beam enables us to use a thin target enough not to deteriorate resolution; these requirements can be met only at HIHR.

In the following section, the physics justification of the measurement will be given.

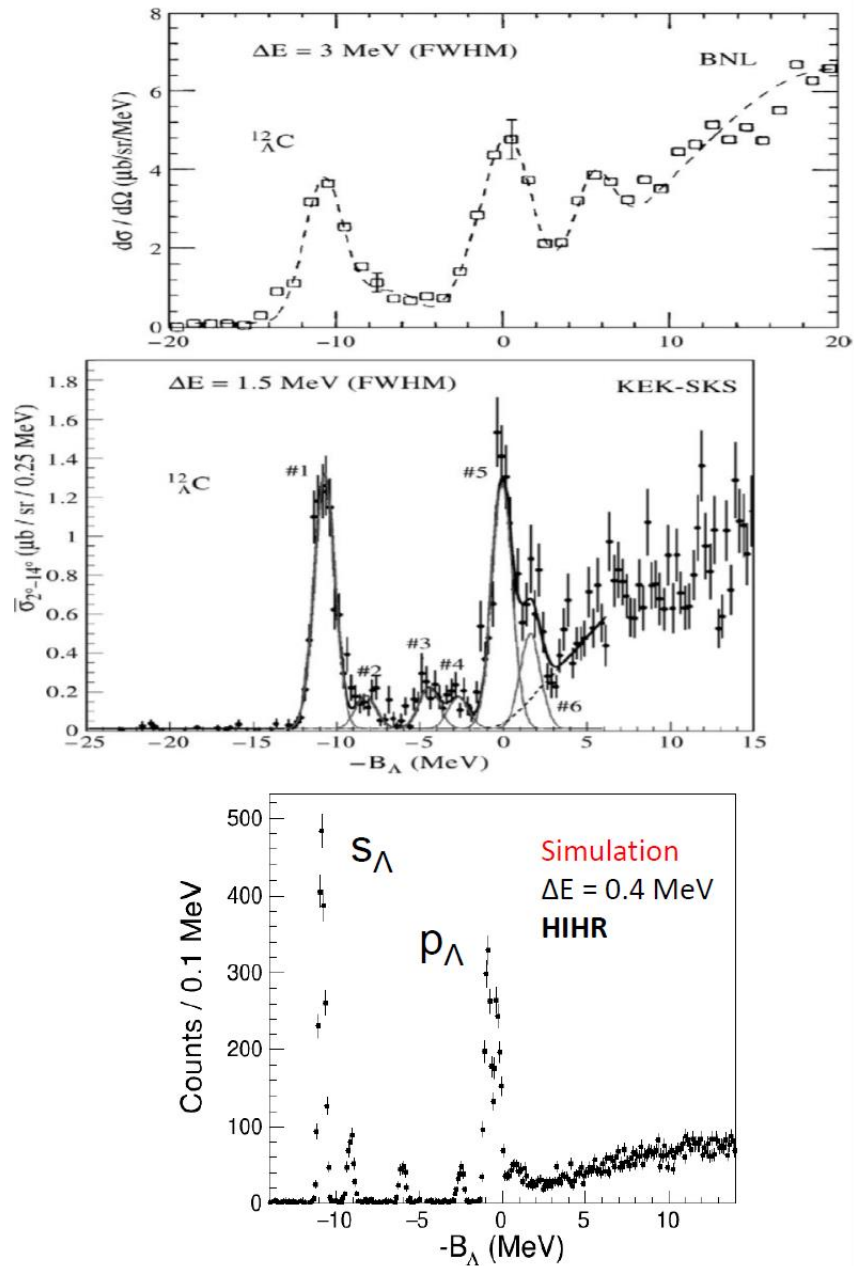


Figure 2-3: Λ binding energy spectra of $^{12}_{\Lambda}\text{C}$ measured at BNL-AGS, KEK-SKS and HIHR(expectation). Simulation for HIHR was carried out based on theoretical calculation for major peaks [MOT10] and quasi-free Λ production events, background events were generated to be consistent with the experimental data [HOT01].

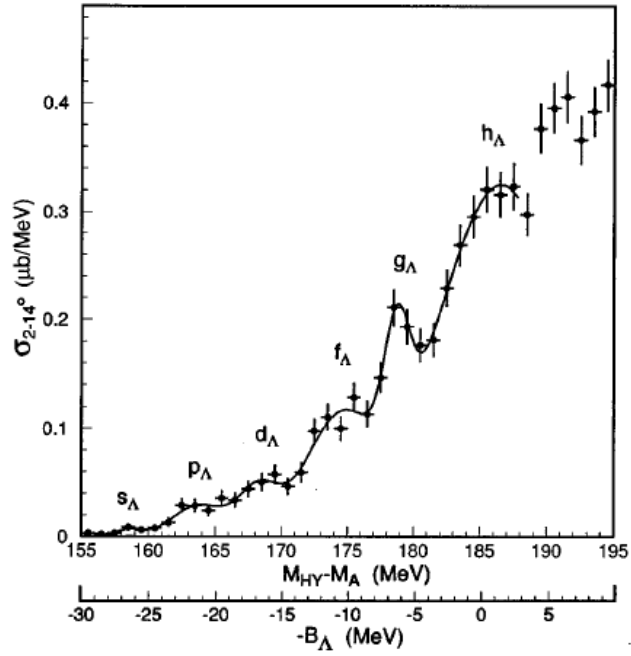


Figure 2-4: Λ binding energy spectra of $^{208}_{\Lambda}\text{Pb}$ measured at KEK-SKS [HAS96]. Major neutron hole series of $(i_{13/2})^{-1}$ with a Λ in s, p, d, f, g, h orbits are barely observed as $s_{\Lambda}, p_{\Lambda}, d_{\Lambda}, f_{\Lambda}, g_{\Lambda}$ and h_{Λ} peaks with an energy resolution of 2.3 MeV.

2.1 Neutron stars and the hyperon puzzle

Neutron stars (NS) are the most compact and dense stars in the universe, with typical masses $M \sim 1.4 M_{\odot}$ and radii $R \sim 10$ km. Their central densities can be several times larger than the nuclear saturation density, $\rho_0 = 0.16 \text{ fm}^{-3}$. Since the Fermi energy of fermions at such densities is in excess of tens of MeV, thermal effects have little influence on the structure of NS. Therefore, they exhibit the properties of cold matter at extremely high densities, very far from being realized in present terrestrial experiments. In the era of multi-messenger astronomical observations, NS offers a unique opportunity to test a broad class of theories, from nuclear physics to general relativity, including the recent observation of gravitational waves [ABB17] and X-ray hotspot measurement by NICER which constraints on mass-radius ratio [PAN21, RAA21]. These recent progresses in astronomical observations have deepened our understanding of **macroscopic features of NS**, such as mass, radius, and stiffness. Therefore, **microscopic understanding becomes more important than ever; we should answer what kind of physics determines the size and mass of NS and why NS is so stiff.**

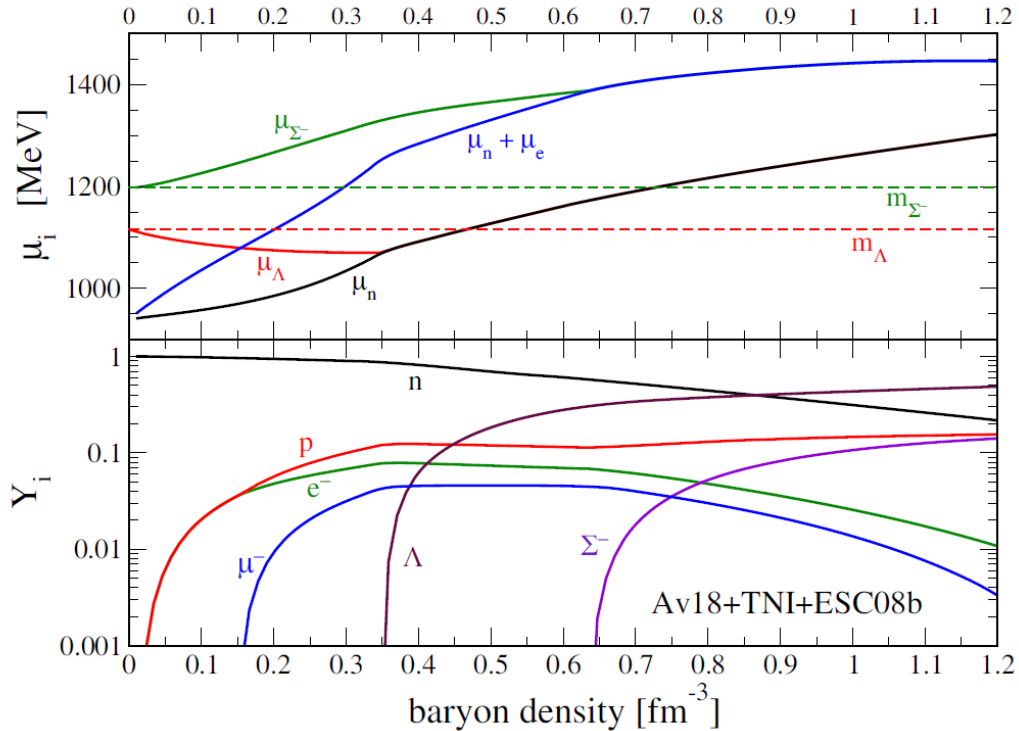


Figure 2-5: Chemical potentials μ , and concentrations Y of the stellar constituents in hyperonic matter as a function of the baryon density [Bom16].

From the surface to the interior of a NS, stellar matter undergoes a number of transitions. From electron and neutron-rich ions in the outer envelopes, the composition is believed to change into a degenerated gas of neutrons, protons, electrons, and muons in the outer core. At densities larger than $\sim 2\rho_0$ new hadronic degrees of freedom or exotic phases are likely to appear. Fig.2-5 shows the chemical potentials and concentrations of stellar constituents in beta-stable hyperonic matter as a function of baryon density, obtained from a recent theoretical calculation employing modern baryonic potentials [Bom16].

The appearance of hyperons in the core of a NS was already advocated in 1960 [AMB60]. In the degenerate dense matter forming the inner core of a NS, Pauli blocking would prevent hyperons from decaying by limiting the phase space available to nucleons. When the nucleon chemical potential is large enough, the conversion of nucleons into hyperons becomes energetically favorable. This results in a reduction of the Fermi pressure exerted by the baryons and a softening of the equation of state (EOS). As a consequence, the maximum mass determined by the equilibrium condition between gravitational and nuclear forces is reduced. The value of about $1.5M_\odot$ for the maximum mass of a NS, inferred from neutron star mass determinations [THO99], was considered the canonical limit, and it was compatible with most EOS of matter containing strangeness. However, the recent measurements of the large mass values of the millisecond pulsars J1614-2230 ($1.97(4)M_\odot$) [DEM10], PSR J0348+0432 ($2.01(4)M_\odot$) [ANT13] and MSP J0740+6620 ($2.14(20)M_\odot$) [CRO19] require a much stiffer equation of state.

This seems to contradict the appearance of strange baryons in high-density matter given what is known at present about the hyperon-nucleon interaction. This apparent inconsistency between NS mass observations and theoretical calculations is a long-standing problem known as “**hyperon puzzle**”. Its solution requires better understanding of the hyperon-nucleon (YN) interaction in a wide range of systems from light to medium and heavy hypernuclei as well as more accurate theoretical calculation frameworks.

Currently there is no general agreement among the predicted results for the EOS and the maximum mass of NS including hyperons. This is due to incomplete knowledge of the interactions governing the system (both two- and three-body forces for hypernuclei) as well as difficulties of theoretical treatment of many-body systems. There are theoretical

calculations which were applied to the hyperonic sector and resulted in the appearance of hyperons at around $2-3\rho_0$, and a strong softening of EOS, implying a sizable reduction of the maximum mass [VID11, HJS11, MAS12]. On the other hand, other approaches suggest much weaker effects arising from the presence of strange baryons in the core of the star [BED12, WEI12, MIY13, LOP14].

Rich nucleon-nucleon (NN) scattering data allow one to derive satisfactory models of two-body nuclear forces, either purely phenomenological [WIR95] or built on the basis of an effective field theory [MAC96, EPE05, EKS13, GEZ13]. In contrast to NN scattering, quite limited scattering data are available for hyperon-nucleon (YN) scattering, though a ΣN scattering experiment was recently performed at J-PARC [MIW11] and a new Λp scattering experiment is planned. Furthermore, there is no scattering data for Λ -neutron and hyperon-hyperon scattering data. The main reasons of this lack of information lie in the short lifetime of hyperons, and the impossibility of collecting hyperon-neutron and hyperon-hyperon scattering data. This implies that realistic hypernuclear interaction models must also rely on information extracted from the binding energies of hypernuclei.

In the non-strange nuclear sector the binding energies of light nuclei have been used to constrain three-nucleon potential models. However, a widely employed phenomenological three-body force (Illinois 7 [PIE08]), while providing a satisfactory description of the spectrum of light nuclei up to ^{12}C [PIE08] yields to an unrealistic EOS for pure neutron matter (PNM) [MAR13]. On the other hand, when additional information on the three-nucleon interaction is inferred from saturation properties of symmetric nuclear matter (Urbana IX force [PUD95]), the resulting PNM EOS turns out to be stiff enough to be compatible with astrophysical observations [GAN12].

Recent analysis of $^{16}\text{O}+^{16}\text{O}$ scattering data shows that the established meson exchange potential model (Nijmegen ESC08c [NAG14]) cannot reproduce the cross section at large scattering angles where density of the system becomes large and inclusion of 3-body force (TBF) solves the problem as shown in Fig. 2-6 [FUR09].

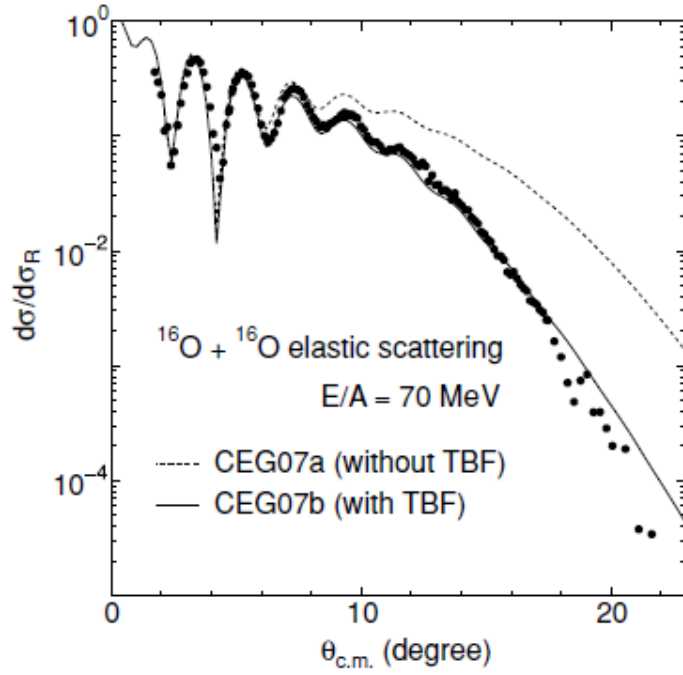


Figure 2-6: Differential cross sections for $^{16}\text{O}+^{16}\text{O}$ elastic scattering at $E/A = 70$ MeV [FUR09].

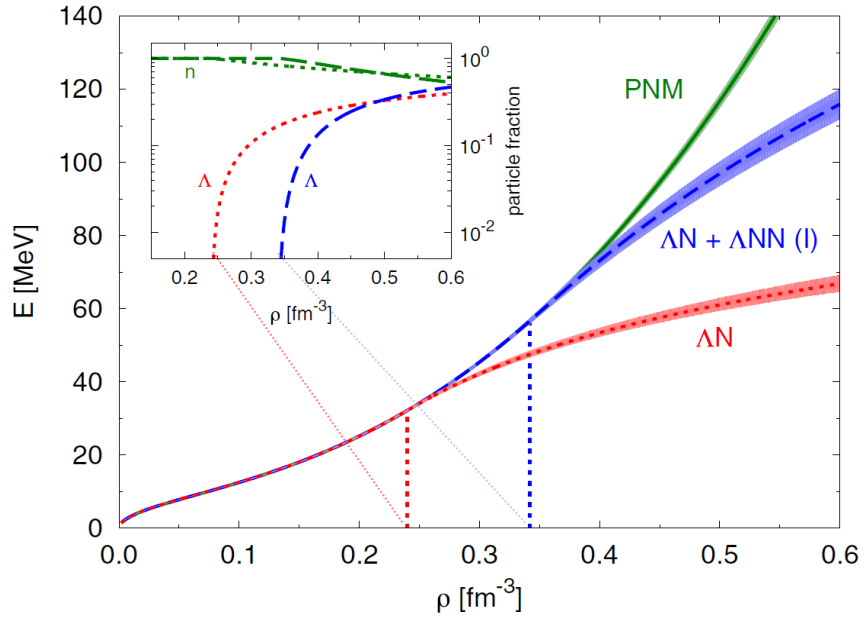


Figure 2-7: Energy as a function of baryon density [LON15]. The vertical dotted lines indicate the Λ threshold densities. In the inset, neutron and Λ fractions correspond to the two hyper-neutron matter EOSs.

It is a quite promising scenario to solve the hyperon puzzle that inclusion of such 3-body repulsive force in the ANN interaction makes EOS harder or prevents cross over of chemical potentials of neutron and Λ to suppress the appearance of Λ in NS.

Figure 2-7 shows one example of EOS of neutron star calculated by quantum Monte Carlo method [LON15]. The EOS of NS without hyperons (Pure Neutron Matter; green) is hard but inclusion of Λ makes the EOS soft (Λ N; red) where density of system becomes higher ($\rho > 1.5 \rho_0 \sim 0.24 \text{ fm}^{-3}$), and inclusion of 3-body repulsive force (blue), stiffness of EOS recovers. Inset plot shows neutron and Λ fractions. One can see that the 3-body repulsive force pushes the Λ appearance threshold up.

Thus, there is a general indication that 3-body repulsive forces become quite significant at high density, and it harden the EOF of neutron stars. The binding energies of light hypernuclei with high statics YN scattering data are necessary to construct realistic YN interaction models, but they are not enough to solve the hyperon puzzle. Additional information must necessarily be inferred from the properties of medium and heavy hypernuclei in order to extrapolate to the infinite-mass limit for discussion of highly massive asymmetric nuclear matter such as neutron stars and strange hadronic matters ($n_u \sim n_d \sim n_s$).

Such information is essential to extrapolate the hyperon behavior to the infinite limit and thus to reliably predict neutron star properties.

2.2 Theoretical models of structure calculation of Λ hypernuclei

Except for very light Λ hypernuclei which ab-initio or detailed cluster calculation can handle, the structure of Λ hypernuclei is generally studied by employing the weak-coupling approximation that assumes the wave function of a Λ hypernucleus to be decomposed into a core nucleus and a Λ hyperon. In this picture, the hypernuclear Hamiltonian consists of the Hamiltonian for the core-nucleus, the Λ kinetic energy and the sum of ΛN interaction terms that can be derived with various theoretical frameworks.

Realistic nuclear interaction models have been constructed based on rich nucleon-nucleon (NN) scattering data but scarce hyperon-nucleon (YN) and completely no YY scattering data limits construction of reliable baryonic interaction models.

Therefore, the analysis of hypernuclear binding energies with the limited number of available hyperon-nucleon (YN) scattering data play key role to formulate various baryon-baryon interaction models. Traditionally, interaction models based on meson exchange picture such as Nijmegen ESC [RIJ10, NAG14, NAG15] and Bonn-Jülich [REU94, HAI05] are widely used. Recently SU(3) chiral effective field theory (ChEFT) [HAI13] attracts attention since it allows improvement of precision of the calculation in systematical way by power counting and two- and three-body forces are derived in a consistent way.

Recent progresses of lattice QCD calculation with massive CPU power computers enable us also to derive the baryonic interaction potential models [AOK10, AOK11, ISH12] and coming closer to a level where they give additional constraints on the baryonic interaction, however, direct calculation of light baryonic systems by lattice QCD is still challenging task.

Ab-initio calculations and microscopic cluster calculations enable us to use these bare interactions to calculate the binding energies of light hypernuclear systems [WIR18, HIY09].

However, analysis of heavier hypernuclei needs effective interactions which have been derived from the bare ΛN force by various calculation techniques such as G-matrix methods based on Bruckner theory [RIJ99] because heavier nuclear systems are too complicated for those microscopic calculations, and it is practically impossible to take all quantum many-body effects into account.

In order to perform theoretical analysis of binding energy information of hypernuclei in wide mass range, following information are necessary: 1) reliable two-body baryonic

interaction, 2) systematic method to convert bare two-body interaction to the effective interaction which takes quantum many body effects adequately into account, and 3) nuclear structure calculation with the derived effective interaction model.

Let us give one example of such calculations: a meson exchange baryon-baryon interaction, ESC08c [RIJ10], which takes two-meson and meson pair exchanges as well as various one boson exchanges into account with broken SU(3) symmetry, is selected as the bare baryon-baryon interaction. As already recognized in the non-strange sector by the study of $^{16}\text{O}+^{16}\text{O}$ scattering data [FUR09], the ESC08c model needs to be supported by a 3/4-body repulsive force originating from multi-Pomeron exchange (MPa) that can be universally extended to the strange sector. Finally, effective YN and YY interaction models were constructed from ESC08c+MPa by Gaussian parametrization of the G-matrices theory in nuclear matter and EOS of neutron star was constructed. Then, Tolmann-Oppenheimer-Volkoff (TOV) equation was solved for the hydrostatic structure and mass-radius relations of neutron stars was obtained[YAM14].

Figure 2-8 shows neutron star masses as a function of the radius. Dotted black curve is for ESC only without three body forces and it was shown that inclusion of hyperon makes EOS very soft. Inclusion of three-body force makes EOS stiffer and maximum mass of NS becomes larger; the case for MPa, two solar-mass NS can be supported.

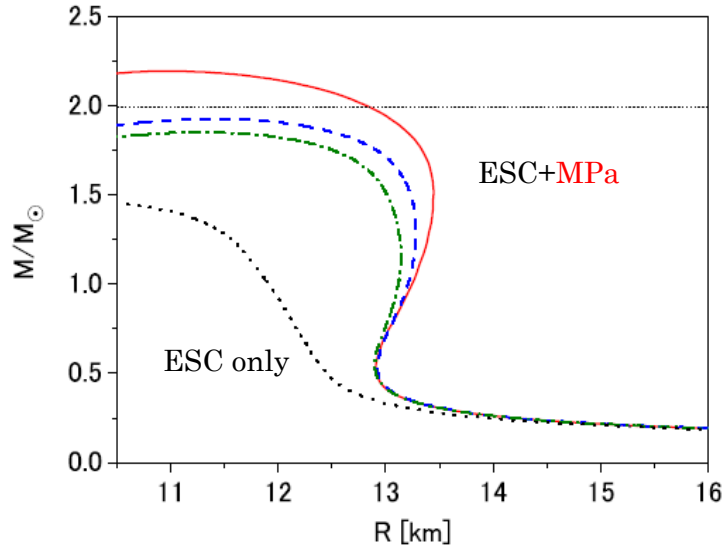


Figure 2-8: Neutron star masses as a function of the radius [YAM14]. Dotted black curve is for ESC only without three body forces and it was shown that inclusion of hyperon makes EOS very soft. Red solid line shows the case with multi-body forces, MPa. Blue and green lines are different parameter set of multi-body forces [YAM14].

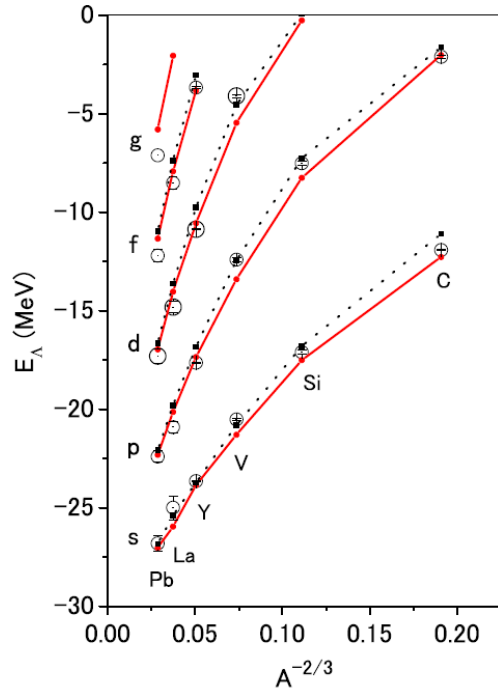


Figure 2-9: Energy spectra of various Λ hypernuclei. Experimental data were marked by open circles and theoretical calculation results with 3-body force (MPa) is red solid line and without 3-body force (ESC) is black dots [YAM14].

Obtaining k_f -dependent local potential derived from the G-matrices calculation for the interaction which recovered the stiffness of NS, hypernuclear energy spectra were calculated with Skyrme Hartree-Fock wave functions (Fig. 2-9). Figure 2-10 shows the effects of three-body force which were obtained from the Λ binding energies in s -orbit with multi-body force (ESC+MPa) and without it (ESC only). Energy differences of the experimental data obtained by previous (π^+ , K^+) spectroscopy and calculated values without multi-body force were plotted, too. Though 3-body force plays a significant role for NS, the effects for hypernuclear energies are small, typically less than 1 MeV. It is clear that the experimental data have too large errors as well as ambiguities to constraint theoretical models. Experiments at HIHR will provide Λ binding energies in wide mass region with an accuracy of < 100 keV. It should be noted that similar discussions for Λ binding energy for p, d, f, \dots -orbits are possible and interaction models are further constrained with those information when reliable Λ binding energies are obtained at HIHR.

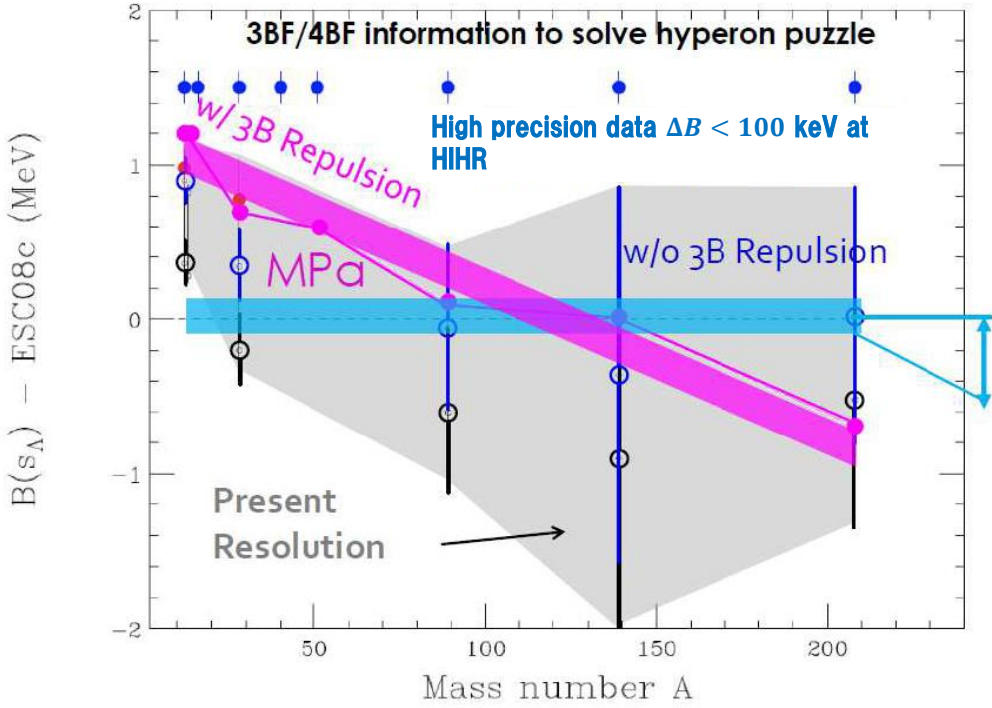


Figure 2-10: Expected effects of 3-body repulsive ANN force for various Λ hypernuclei [YAM14]. Open black circles are previous data obtained by previous (π^+ , K^+) spectroscopy of Λ hypernuclei. Recently possible ambiguity of 0.5 MeV was pointed out [GOG16, BOT17] for all these data and blue circles shows the experimental data with this ambiguity. Expected precision of experiments at HIHR was shown by error bars of closed circles.

There are variety of theoretical calculations depending on choice of bare interactions and treatment of quantum many-body problem.

The effective G-matrix potential from the Nijmegen potential including many-body force was combined with a microscopic calculation, Hyper-AMD to calculate the binding energies of ${}^{12}_{\Lambda}\text{B}$, ${}^{13}_{\Lambda}\text{C}$, ${}^{16}_{\Lambda}\text{O}$, ${}^{28}_{\Lambda}\text{Si}$, and ${}^{51}_{\Lambda}\text{V}$ [ISA16, ISA17].

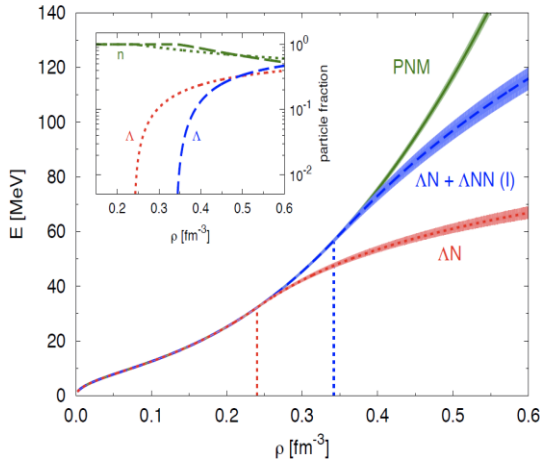
The different version of Nijmegen potential with Pomeron and Odderon exchanges (ESC16) with the G-matrix calculation [NAG19] was also carried out.

Recently, the auxiliary field diffusion Monte Carlo (AFDMC) technique for strange systems has made substantial progresses. By using this microscopic ab-initio approach, an accurate analysis of the Λ separation energy of light- and medium-heavy hypernuclei has been carried out [LON14, PED15] using a phenomenological interaction [BOD84, USM95, IMR14] in which the two-body potential has been fitted on the existing Λp scattering data.

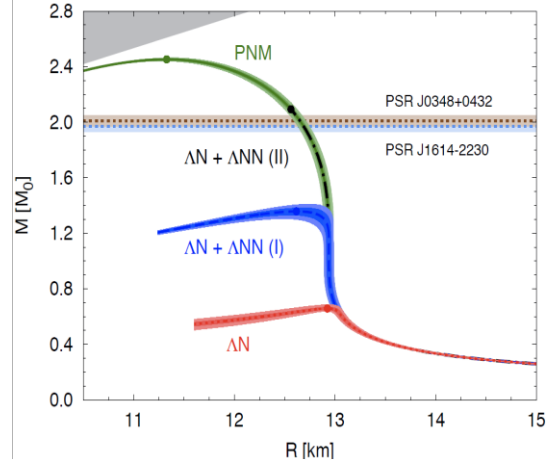
As shown in Fig.2-11(a), when only the two-body ΛN force is considered (red curve), the calculated hyperon separation energies tend to disagree with the experimental data (green curve) as the density increases. This has a sizable effect on the predicted NS structure, Fig. 2-11(b).

The inclusion of the three-body ΛNN force in this scheme leads to a satisfactory description of the hyperon separation energies in a wide mass range and for the Λ occupying different single particle state orbitals (s , p and d wave), as shown in Figs. 2-12(b). The resulting EOS spans the whole regime extending from the appearance of a substantial fraction of hyperons at $\sim 2\rho_0 \simeq 0.32 \text{ fm}^{-3}$ to the absence of Λ particles in the entire density range of the star, as shown in Fig. 2-12(a).

Recently SU(3) Chiral Effective Field Theory (ChEFT), which based on chiral symmetry of QCD Lagrangian, attracts wide attention [POL06, PET16, KOH18, HAI20]. ChEFT established a prescription to extend the interaction model to include many-body forces. Performed next-to-leading order (NLO) calculations already included some components of the 3-body force (the ones that can be reduced to 2-body terms), but next-to-next-to-leading order (NNLO) calculations are necessary for the inclusion of a genuine 3-body interaction, and more experimental inputs such as high statistics YN scattering data to be available at K1.1 beamline of J-PARC extended hadron hall and high precision binding energy information of light hypernuclei, are required to constraint the Low-Energy Constants which are necessary parameters to make ChEFT predictable.

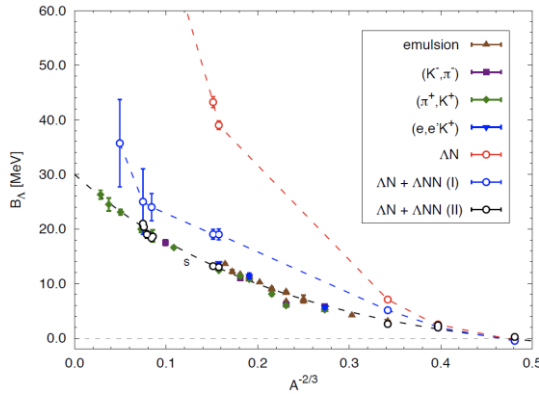


(a) Equations of state. The vertical dotted lines indicate the Λ threshold densities. In the inset, neutron and Λ fractions correspond to the two hyperneutron matter EOSs.

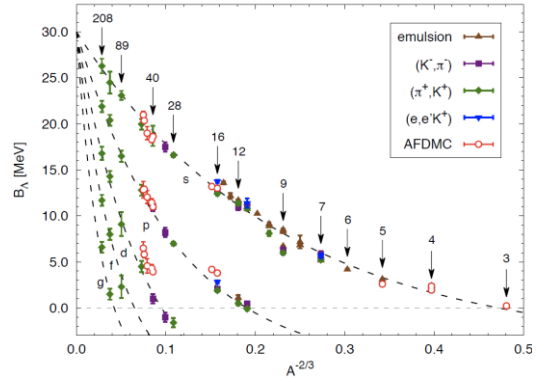


(b) Mass-radius relations given by AFDMC. Closed circles represent the predicted maximum masses. Horizontal bands at $2M_{\odot}$ are the observed masses of the heavy neutron stars [DEM10, ANT13].

Figure 2-11: EOS and neutron star mass-radius relations calculated by AFDMC [LON15].



(a) Experimental B_{Λ} values in s wave and AFDMC calculation results with 2-body ΛN interaction alone, and two different parametrizations of the 3-body YN interaction (updated from [LOD14]).



(b) Experimental results for Λ in s, p, d, f and g waves. Red open circles are the AFDMC results obtained including the most recent 2-body plus 3-body hyperon-nucleon phenomenological interaction model (updated from [PED15]).

Figure 2-12: Λ separation energies as a function of $A^{-2/3}$. calculated by AFDMC

Although the above calculations are based on different bare potentials: meson exchange Nijmegen potential, phenomenological one or ChEFT, and they adopt different approaches how to apply these potentials to hypernuclei: G-matrix calculation, microscopic ab-initio quantum Monte Carlo calculation, the general tendencies of results are consistent.

They predict that inclusion of 3-body repulsive force makes relatively small differences in the Λ separation energies of hypernuclei but it gives dramatically different results for the properties of the infinite medium like a NS: hardening of EOS or even suppression of the hyperon appearance [YAM14, LON15, GER20].

However, while 2-body baryonic force models based on different theoretical frameworks are expected to be reasonably accurate from new data of YN scattering at K1.1 J-PARC and information of light hypernuclei, detailed information on the 3-body hyperon-nucleon interaction is still missing. This lack of knowledge is to be attributed to a poor experimental information for medium to heavy hypernuclei, which are the key to infer properties of the infinite hyper-nuclear matter. Therefore, in order to properly assess the role of hyperons in NSs and reconcile theoretical predictions with astrophysical observations, *i.e.* solve the hyperon puzzle, precise experimental investigation on light, medium and heavy targets is of paramount importance. In order to provide such accurate experimental data efficiently, realization of HIHR beamline is essential.

2.3 Choice of targets, additional physics outputs

Other proposals for wide variety of targets will follow after the success of the proposed experiment but let us limit the choice targets for the first campaign of hypernuclear research at HIHR for now.

As shown in Fig. 2-10, 3-body force effect depends on mass number of hypernuclei, choice of targets should cover wide mass range from light to heavy targets. As discussed in section 5, thin targets are necessary to realize a high-resolution experiment. Therefore, self-supporting solids targets with a thickness of about millimeters were chosen for the first campaign of hypernuclear experiments at HIHR. Surely, **the main goal of the proposed experiment is to solve the hyperon puzzle by systematic study of Λ hypernuclei in wide mass range, but physics outputs of high resolution spectroscopy of Λ hypernuclei are not limited to that.**

So far ^{12}C target was used as a reference for the (π^+, K^+) spectroscopy of hypernuclei due to its easy handling. Because the proposed experiment would be the first experiment at HIHR, beamline commissioning including dispersion matching parameters' optimization will be carried out.

Li, Be, B targets can be prepared as self-supporting targets and they are theoretically within scope of precise few body calculation techniques, such as microscopic cluster model [HIY09] and no-core shell model calculation which was extended to $^7_\Lambda\text{Li}$ for hypernuclei [LE20] and to ^{12}C for normal nuclei [NAV00].

Importance of $\Lambda\text{N}-\Sigma\text{N}$ coupling is widely recognized for discussion of Charge Symmetry Breaking (CSB) of Λ hypernuclei [HIY01,GAZ16,NOG19]. For heavier and neutron richer hypernuclear systems, such $\Lambda\text{N}-\Sigma\text{N}$ coupling and 3-body force become more important, implying that the behavior of Λ in symmetric nuclear matter and neutron-rich environments would be quite different. It was pointed out that the $\Lambda\text{N}-\Sigma\text{N}$ coupling is quite important also for the discussion of NS [HAI07].

Since there is high resolution (< 1 MeV resolution) spectroscopic experiments with electron beams for $^7_\Lambda\text{He}$ [NAK13,GOG16-2], $^9_\Lambda\text{Li}$ [GOG21] and $^{10}_\Lambda\text{Be}$ [GOG16] at JLab, and thus measurement of their isospin multiplet partners, $^7_\Lambda\text{Li}$, $^9_\Lambda\text{Be}$ and $^{10}_\Lambda\text{B}$ are important to study with same or better energy resolution at HIHR; such precise data will enable us to discuss CSB and the $\Lambda\text{N}-\Sigma\text{N}$ coupling in detail.

The region of medium mass hypernuclei is also interesting. Precision measurement of them will clarify the single-particle behavior of a Λ hyperon in the nuclear system, investigation of baryonic many-body system with strangeness degree of freedom, and the effective Λ -N interaction.

Dynamics of a core nucleus, which is a many-body system of protons and neutrons, couples to a Λ hyperon motion which is free from Pauli effects of nucleons, and then new symmetric states, “genuine hypernuclear states”, will appear [MOT21, ISA13]. Deformation of nuclei can be studied by measuring these states.

Though recent progresses of microscopic calculations such as Hyper-AMD [ISA17] and AFDMC [LON14] make it possible to discuss medium-heavy hypernuclei, the mean-field picture is also important.

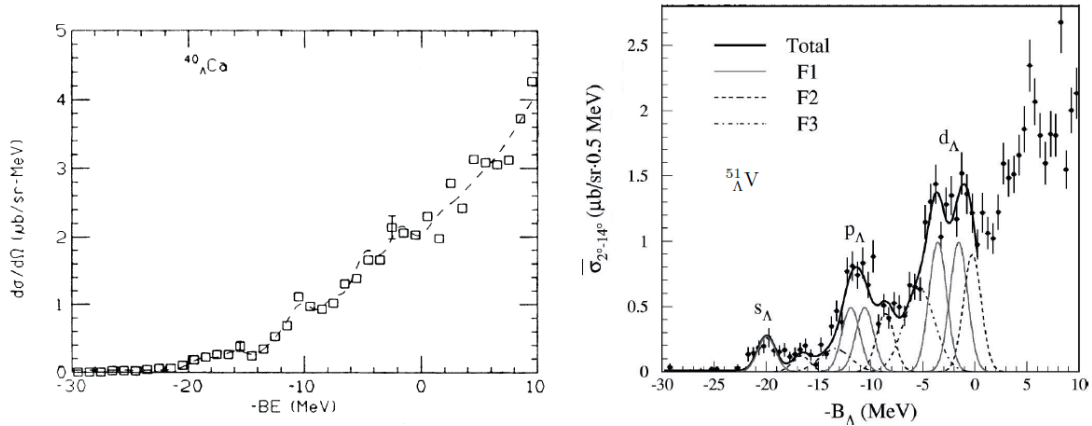


Figure 2-13: $^{40}_{\Lambda}\text{Ca}$ [PIL91] and $^{51}_{\Lambda}\text{V}$ [HOT01] spectra obtained by the (π, K) reaction.

In the investigation of hadronic many-body systems with strangeness, there is a fundamental question, “to what extent does a Λ hyperon keep its identity as a baryon inside a nucleus?” [YAM84]. Spectroscopic data in heavier hypernuclei can help to answer this question. Indeed, the relevance of the mean-field approximation in nuclear physics is one of the prime questions related to the role that the sub-structure of nucleons plays in the nucleus. The mean-field dynamics dominates the structure of medium to heavy nuclei and Λ hypernuclei prove the existence of single-particle motion from the deepest s -orbit up to large Λ valence orbits. The existing data from (π^+, K^+) reactions obtained at KEK, however, do not resolve the fine structure in the missing mass spectra due to limited energy resolution, and theoretical analyses suffer from those uncertainties as shown in Fig. 2-13. The improved

energy resolution at HIHR, which is comparable to the spreading widths of the excited hypernuclear states, will provide wide variety of information. For example: 1) differentiation between the effects of the static spin-orbit potential and dynamical self-energies due to core polarization; 2) access to collective motion of the core nucleus, namely deformation of the core nucleus, utilizing the Λ as a probe; 3) modify energy levels of a core nucleus by adding a Λ as an impurity and so on.

Effective masses of a Λ hyperon in the nuclear potential will be obtained, which appear to be closer to that of the free value in contrast to the case of ordinary nuclei. Therefore, the proposed precision measurement of the single particle levels can address the degree of non-locality of the effective Λ -Nucleus potential and can be compared, for example, with the advanced mean field calculations based on the quark-meson coupling (QMC) model [TSU98] and on DDRH [KEI00]. This can be related to the nature of the ΛN and ΛNN interactions, and to the ΛN short range interactions [MOT88]. In a more exotic way, the binding energies were discussed in terms of the distinguishability of a Λ hyperon in the nuclear medium, which will result in a different A dependence of the binding energy as suggested by Dover [DOV87].

Lead target is a *holy grail* for the Λ hypernuclear spectroscopy. The ^{208}Pb nucleus is doubly magic nucleus and heaviest target which can be easily available as a self-supporting plate. Its charge density distribution is nearly constant for a very large fraction ($\sim 70\%$) of the nuclear volume as shown in Fig. 2-14 [FRO87], and its properties were expected to reflect those of uniform nuclear matter.

List of targets for the proposed experiment will be compiled in section 6 with the requesting beamtime.

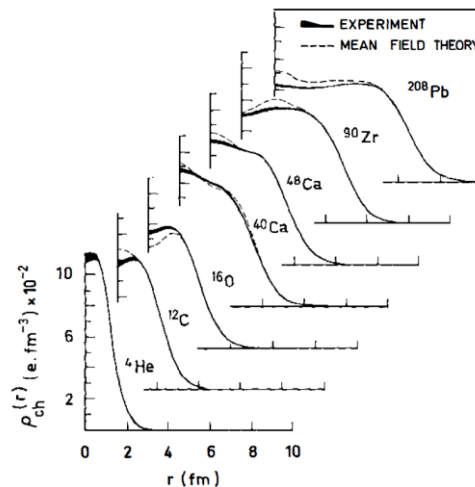


Figure 2-14: Charge density distribution of doubly closed-shell nuclei [FRO87].

2.4 International competition and cooperation

There are growing efforts worldwide in hypernuclear spectroscopy and following projects are on going:

1. JLab has a campaign of hypernuclear physics programs to investigate isospin and mass dependence of Λ hypernuclei with electron beams. The energy resolution of the $(e, e'K^+)$ reaction spectroscopy is 0.5 – 1.0 MeV (FWHM) and its energy resolution is comparable to it of HIHR. However, the $(e, e'K^+)$ reaction converts a proton to a Λ , while the (π^+, K^+) reaction converts a neutron to a Λ , and thus produced hypernuclei are different species. Therefore, detailed comparison between hypernuclei produced by (π^+, K^+) and $(e, e'K^+)$ reactions from the same target will give direct information about Charge Symmetry Breaking. So far, resolution of previous (π^+, K^+) experiments do not match to it of $(e, e'K^+)$, and thus detailed comparison was impossible. JLab hypernuclear program could be a strong competitor as well as a strong collaborator. It should be noted there are lots of backlog of accepted experiments at JLab and installation/decommission of major spectrometers take a quite long time (from a few months to a half year). Frequent beamtime assignment is difficult at JLab.
2. MAMI has an electron microtron which can produce strangeness and the similar hypernuclear programs to JLab can be performed in principle. However, it is unlikely that the $(e, e'K^+)$ reaction spectroscopy will be conducted on a large scale, due to limitation of the existing kaon spectrometer. Decay π spectroscopy of electro-produced hypernuclei was successfully carried out for ${}^4_\Lambda\text{H}$ and the kaon spectrometer at MAMI serves perfectly as a kaon tagger for this experiment. Though measurements are limited only to ground states of light hypernuclei, decay π spectroscopy's energy resolution is 0.15 MeV (FWHM). Though there are experimental plans to perform decay pion spectroscopy at HIHR [FUJ21], MAMI has already established high-resolution spectrometers for 90-130 MeV/c π 's. MAMI is a quite strong competitor on spectroscopy of ground states of light hypernuclei.
3. GSI-HypHI, RHIC-STAR and LHC-ALICE have started spectroscopic studies of hypernuclei with heavy ion beams. HI hypernuclear spectroscopy attracts attention because it can produce highly exotic hypernuclei, such as proton-rich or neutron-rich hypernuclei which are out of reach by standard spectroscopic techniques. Future experiments at FAIR/GSI are planned also for light hypernuclei. Although it is a

promising and practically only program to access highly exotic hypernuclei, they cannot be competitor for HIHR in terms of energy resolution and signal-to-ratio. FAIR-PANDA is planning a spectroscopy of multi-strangeness hypernuclei with a gamma-ray measurement by using anti-proton beams. Ultimate physics goal of link between QCD and nuclear physics might be shared with HIHR, but experimental technologies are totally different and it cannot be a direct competitor for HIHR.

For the past decade, J-PARC has been a major player in hypernuclear research. Maintaining current activities for the next decade is not enough for J-PARC. Early realization of HIHR and exploring new possibilities of the (π^+, K^+) reaction spectroscopy are essentially important to keep our international competitiveness.

3. Experimental Setup

3.1 High Intensity High Resolution Beamline

The proposed experiment is to perform the high precision mass spectroscopy of Λ hypernuclei produced by the (π^+, K^+) reaction and will employ a newly designed momentum dispersion matching pion beamline and kaon spectrometer, the High Intensity High Resolution beamline (HIHR) which is schematically illustrated in Fig. 3-1.

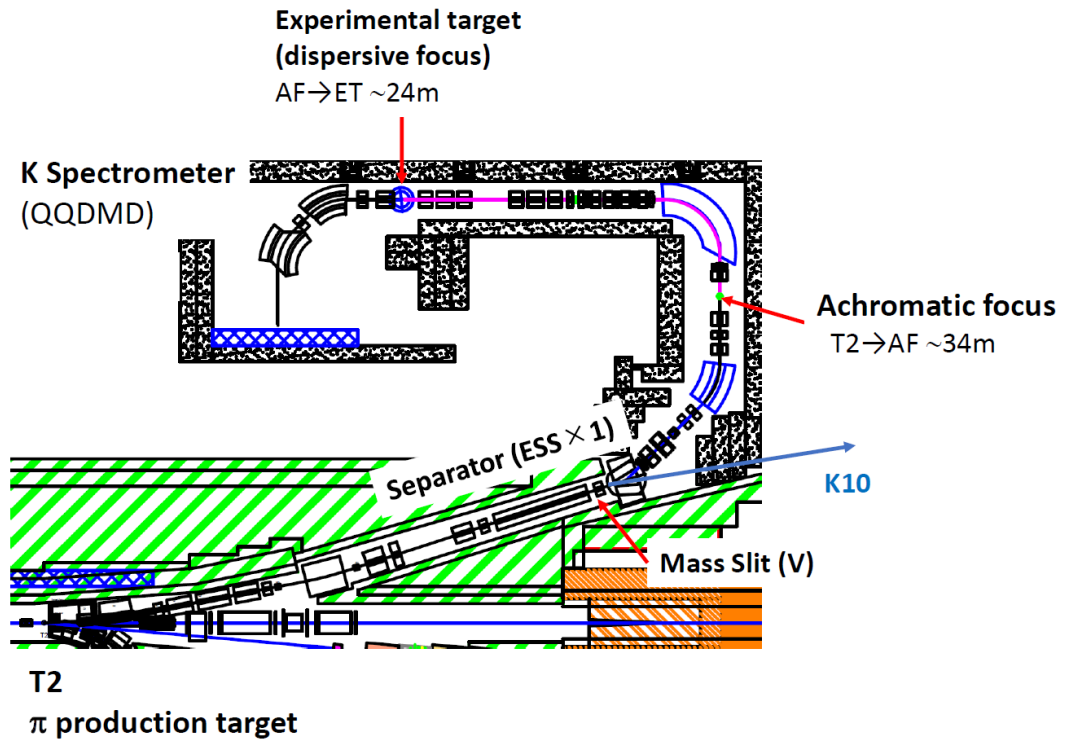


Figure 3-1: Schematic illustration of the High Intensity High Resolution beamline with a kaon spectrometer.

The high intensity, high resolution beamline (HIHR) ion-optically realizes a strongly correlated beam in position and momentum. Combining a properly designed kaon spectrometer to HIHR, which is the so-called dispersion matching ion-optical technique, as described below, one can carry out high-precision spectroscopy in nuclear physics. In particular, Λ -single particle energies in various Λ hypernuclei can be measured at an energy resolution of as high as a few hundred keV which enables us to determine Lambda binding energy with an accuracy of <100 keV.

As the dispersion matching beamline does not require a beam measurement, one can remove

beamline detectors and reduce beamline materials that affect the energy resolution due to multiple scattering and momentum straggling effects. HIHR provides a solution to utilize full-intensity beams potentially available at J-PARC, while available beam intensity would be limited a capability of detectors used as beam counters in usual beamlines.

Detailed description of the momentum match technique will be given in section 3.3.

HIHR is composed of 4 sections as explained below. In the most upstream section, the secondary particles produced at the primary target are collected at the production angle of 3 degrees. The maximum momentum of the secondary beam is designed to be 2 GeV/ c . The base design of the spectrometer follows it of K1.8 beamline in the current hadron hall [AGA12] and the beamline layout of the extraction part would be essentially the same as that of K1.8. The secondary beam is focused vertically at the intermediate focal (IF) point. The secondary beam image is redefined here by the IF slit placed.

In the second section after the IF point, a pion beam is separated from the other particle beams. In this section, by using two sets of a pair of quadrupole magnets (Q-doublet), a so-called point-to-point ion-optics in the vertical direction is realized between the IF point and the MS point at the end of this section. An electrostatic separator (ESS) having a pair of parallel plate electrodes of 10 cm gap and 4.5 m long is placed between the Q-doublets.

Charged particles are kicked vertically by an electrostatic field produced in the ESS. One can compensate the vertical kick by the pitching magnets placed just before and after the ESS. While the kicked angle by the ESS is proportional to the inverse of the particle velocity, the kicked angle by the magnets is proportional to the particle momentum, Namely, a particle beam compensated its kicked angle keeps the beam level and the other particle beams not fully compensated their kicked angles are focused at the different positions in vertical at the MS point. A mass slit (MS) is placed at the MS point so as to select a particle beam and block the other unwanted particle beams.

In the third section after the MS point, the secondary beam is focused achromatically in the horizontal and vertical directions at the IF2 point (Achromatic focus in Fig. 3-3). The beam profile is defined again by the beam slits placed at the IF2 point. In the final section after the IF2 point, by placing a large bending magnet and a several quadrupole magnets, the beam is focused with a magnification of 1.1 and a dispersion of 11 [cm/%] at the experimental target. Here, ion-optical aberrations to the second order are eliminated by

three sextupole magnets.

Overall, this experimental design is for (1) the highest possible resolution (<400 keV FWHM) to determine Λ binding energies with an accuracy of <100 keV, (2) the highest reachable yield with the high intensity π^+ beam, in the reaction spectroscopic study of hypernuclei.

3.2 Kinematics and key parameters of HIHR beamline and spectrometer

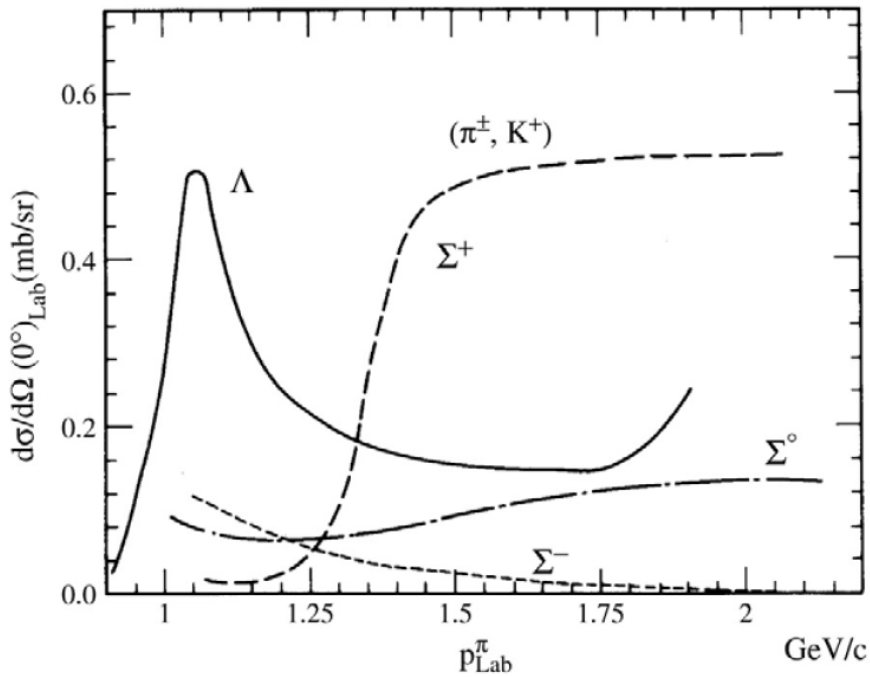


Figure 3-2: The hyperon production cross section as a function of incident pion momentum [HAS06].

The proposed kinematics is assuming use of a pion beam momentum of $p = 1.05$ GeV/ c , where the cross section of the elementary process becomes maximum as shown in Fig. 3.2 . For the ${}^A Z(\pi^+, K^+) {}^A_\Lambda Z$ reaction, the central momentum of the kaon spectrometer is determined to be 0.72 GeV/ c . if the π^+ beam momentum is set at 1.05 GeV/ c .

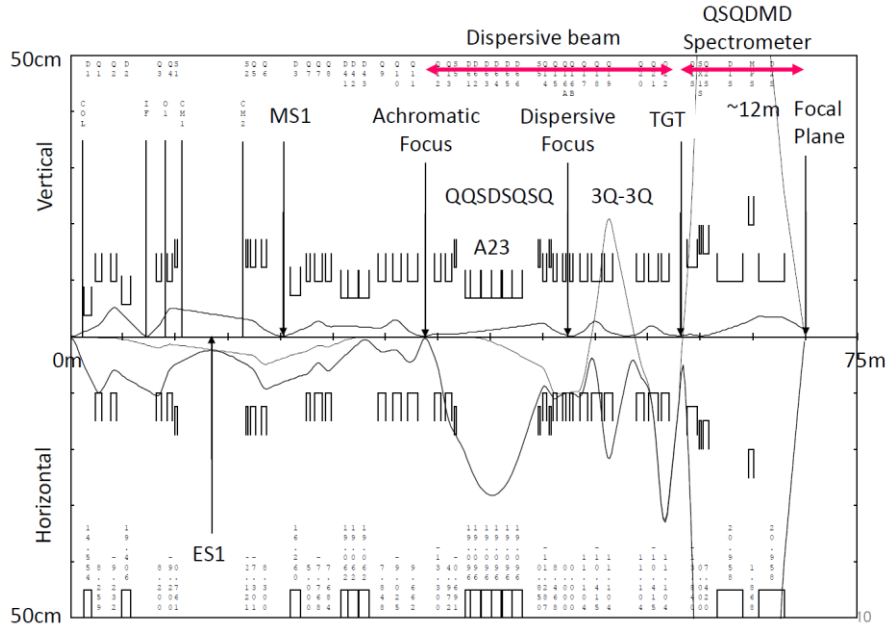


Figure 3-3: The layout of HIHR magnets and calculated beam envelope with TRANSPORT [NOU19].

The layout of HIHR magnets and calculated beam envelope are shown in Fig.3-3. Though detailed design of HIHR beamline highly depends on the design of primary target and beam extraction part which will be shared with the other beamlines in the hadron extension hall, optical features of the π beamline and K spectrometer were studied with a GEANT4 Monte Carlo simulation (Fig. 3-4) based on conceptual design [NOU19] of HIHR calculated by an optics optimization code, TRANSPORT.

The kinematic and key parameters for the current design of HIHR estimated by the GEANT4 simulation with the 2nd order matrix tune are summarized in Table 3-I.

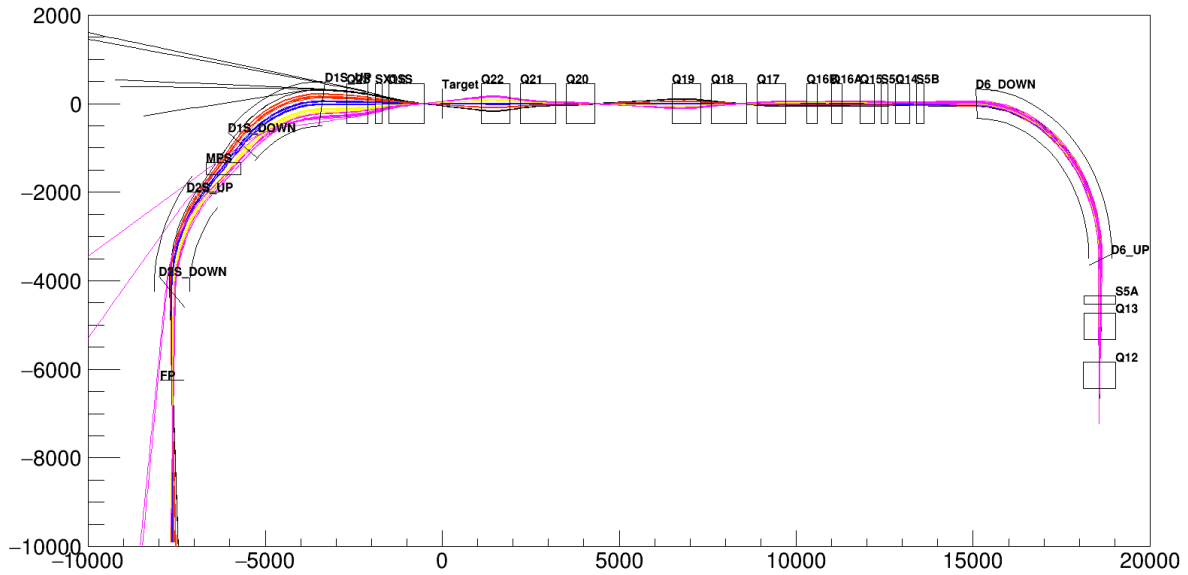


Figure 3-4: GEANT4 model of the HIHR beamline after the achromatic focus point (IF2) and the kaon spectrometer. Unit of scale is millimeter.

Table 3-I: Parameters of the HIHR beamline (GEANT with 2nd order matrix tune)

| | |
|--|-----------|
| Beam π^+ central momentum | 1.1 GeV/c |
| Total length (m) from achromatic focus to the experimental target. | 24.8 |
| Momentum acceptance (%) | ± 1 |
| Horizontal magnification | -1.13 |
| Vertical magnification | -0.88 |
| Dispersion (cm/%) | 11.28 |

Table 3-II: Parameters of the HIHR kaon spectrometer (GEANT with 2nd order matrix tune)

| | |
|------------------------------|------------|
| K^+ central momentum | 0.71 GeV/c |
| Total length (m) | 11.4 |
| Horizontal acceptance (mrad) | ± 60 |
| Vertical acceptance (mrad) | ± 100 |
| Momentum acceptance (%) | ± 5 |
| Horizontal magnification | -1.84 |
| Vertical magnification | -0.54 |
| Dispersion (cm/%) | 10.72 |

3.3 Beamline and K spectrometer dispersion match setting

The kaon spectrometer matched to HIHR beamline comprises the QSQDMD configuration, where D, Q, S, and M stand for a dipole, a quadrupole, a sextupole, and a multipole magnet, respectively. A dispersion matching ion optical technique [SJO60, FUJ97, FUJ99] is a well-established technique for long-living ions, but there has been no application to the secondary meson GeV beamline.

Applying this technique to the secondary π^+ beamline with high-resolution kaon spectrometer, a Λ hypernuclear energy spectrum can be obtained in the (π^+, K^+) reaction by measuring K^+ position distribution at the final focal plane of the kaon spectrometer.

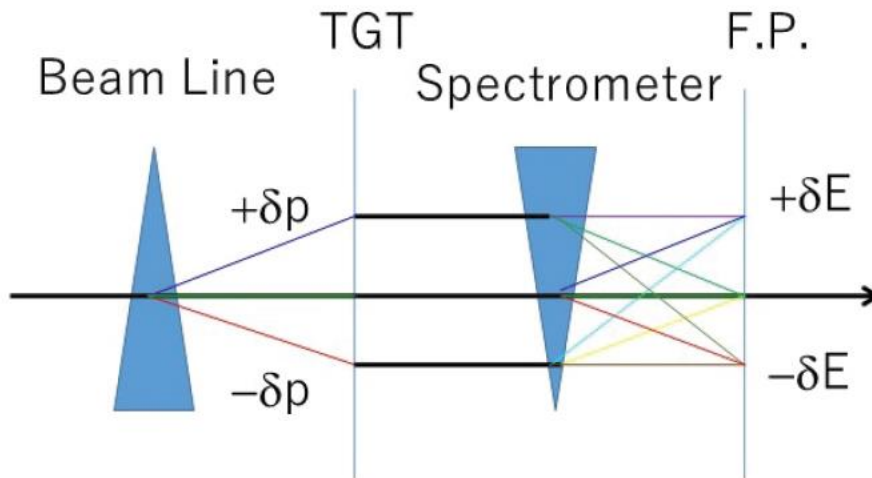


Figure 3-5: Conceptual illustration of momentum dispersion matching.

Fig. 3-5 shows a conceptual illustration of the momentum dispersion matching technique. Secondary π^+ is transferred from the primary target with a momentum bite of $\pm 1\%$, which corresponds to $\pm 11 \text{ MeV}/c$. Therefore, it is essential for sub-MeV spectroscopy to measure their momentum, one by one if a conventional beamline is used. Limitation of beam rate for beam detectors does not allow us to use very high intensity beam. In the momentum dispersion matching beamline, the beam momentum spread is converted to beam position distribution on the target where (π^+, K^+) reaction takes place (Fig. 3-6). Kaon

spectrometer's dispersion and magnification are adjusted to cancel the beamline's momentum dispersion.

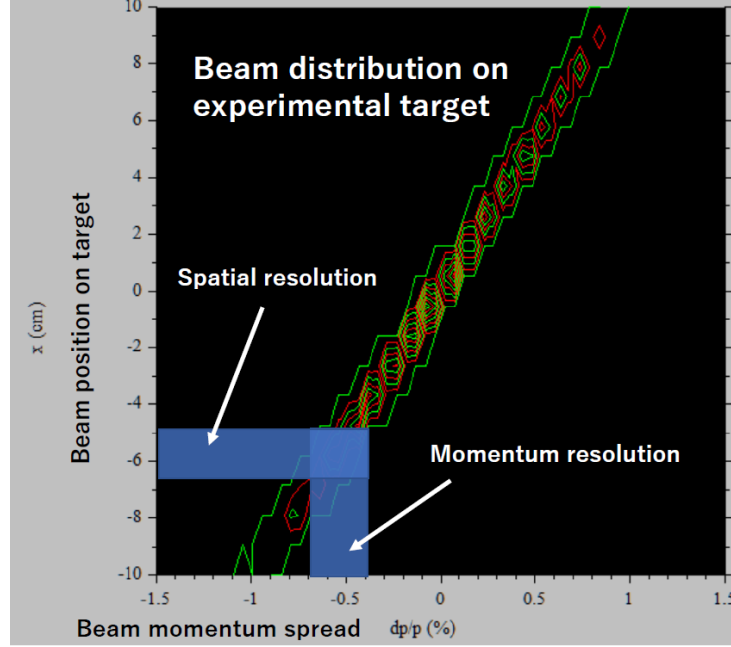


Figure 3-6: π beam momentum spread is converted to beam position spread on the experimental target. Beam distribution was calculated with a beam optics code, TRANSPORT. Momentum spread of 1% is converted to spatial beam spread of 10 cm.

Let us explain how the dispersion match conditions are realized.

The first order beam transfer matrix is given as follows with the initial coordinate $(x_0, \theta_0, \delta_0)$, position, angle and relative momentum with respect to the central momentum and $(x_f, \theta_f, \delta_f)$ for them at the final point.

$$\begin{pmatrix} x_f \\ \theta_f \\ \delta_f \end{pmatrix} = \begin{pmatrix} s_{11} & s_{12} & s_{16} \\ s_{21} & s_{22} & s_{26} \\ 0 & 0 & 1 \end{pmatrix} \begin{pmatrix} T & 0 & 0 \\ 0 & \frac{\theta}{\theta_1} + 1 & 0 \\ 0 & 0 & \frac{K\theta + DQ}{\delta_0} + C \end{pmatrix} \begin{pmatrix} b_{11} & b_{12} & b_{16} \\ b_{21} & b_{22} & b_{26} \\ 0 & 0 & 1 \end{pmatrix} \begin{pmatrix} x_0 \\ \theta_0 \\ \delta_0 \end{pmatrix}$$

$$\theta_1 = b_{21}x_0 + b_{22}\theta_0 + b_{26}\delta_0,$$

$$K = \left(\frac{\partial p_{scat}}{\partial \theta} \right) \left(\frac{1}{p_{scat}} \right),$$

$$C = \left(\frac{\partial p_{scat}}{\partial p_{beam}} \right) \left(\frac{p_{beam}}{p_{scat}} \right),$$

$$D = \left(\frac{\partial p_{scat}}{\partial Q} \right) \left(\frac{1}{p_{scat}} \right),$$

Here, T , θ and Q are a cosine of an angle between a beam direction and a normal to a target plane, a scattering angle, and an excitation energy, respectively. Values of K and C are respectively a derivative of the scattered momentum (p_{scat}) to the scattering angle (θ) and that to the beam momentum (p_{beam}). D is a derivative of p_{scat} to Q .

The position x_f at the final focal plane of kaon spectrometer can be expressed as:

$$x_f = \left(\frac{\partial x_f}{\partial x_0} \right) x_0 + \left(\frac{\partial x_f}{\partial \theta_0} \right) \theta_0 + \left(\frac{\partial x_f}{\partial \delta_0} \right) \delta_0 + \left(\frac{\partial x_f}{\partial \theta} \right) \theta + s_{16} D Q.$$

Lateral dispersion match condition can be written as:

$$\left(\frac{\partial x_f}{\partial x_0} \right) = s_{11} b_{11} T + s_{12} b_{21} \rightarrow \text{minimize},$$

$$\left(\frac{\partial x_f}{\partial \theta_0} \right) = s_{11} b_{12} T + s_{12} b_{22} \rightarrow 0,$$

$$\left(\frac{\partial x_f}{\partial \delta_0} \right) = s_{11} b_{16} T + s_{12} b_{26} + s_{16} C \rightarrow 0,$$

$$\left(\frac{\partial x_f}{\partial \theta} \right) = s_{12} + s_{16} K \rightarrow 0.$$

Fixing reaction kinematics and a scattering angle, magnetic component of beamline and spectrometers are tuned to satisfy the above conditions. Degrees of freedom to be tuned in beamline and spectrometer systems are 6 and 3, respectively.

Once the matching conditions are satisfied, the excitation energy Q can be given as $x_f / (s_{16} D)$ with an energy resolution of $(\partial x_f / \partial x_0) x_0$. In the real operation of the beamline, higher order terms of matrices should be taken into account and the momentum matching parameter optimization will be performed with an established parameter minimization algorithm on the computer.

3.4 Detectors for the kaon spectrometer

Detection of $0.7 \text{ GeV}/c \text{ K}^+$ is possible with well-established experimental techniques. Detector package based on it of SKS in K1.8 [TAK12] can be adopted, namely a plastic scintillation counter for time-of-flight measurement, aerogel and lucite Cherenkov counters for kaon identification at the trigger level and a drift chamber system to measure positions and angles of K^+ s at the focal plane of the spectrometer. As discussed in section 5, position resolution of 0.2 mm (rms) which was achieved by the SKS detector is good enough for the tracking devices at HIHR.

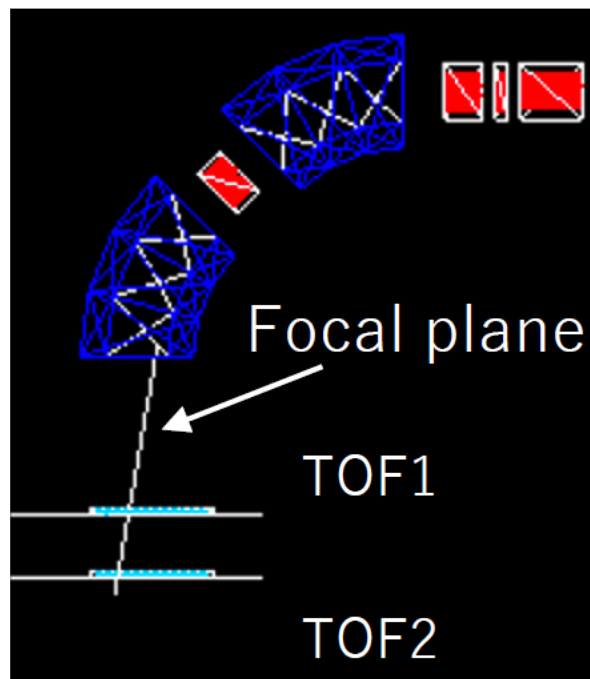


Figure 3-7: A set of plastic scintillation walls are placed just downstream of the focal plane in GEANT4 simulation model (detailed discussion about GEANT4 simulation will be given in section 5).

Figure 3-7 shows a set of plastic scintillation walls placed just downstream of the kaon spectrometer's focal plane with a distance of 1 meter. Particle hit position distribution was estimated with GEANT4 simulation. From the hit position distribution shown in Fig. 3-8, TOF walls should cover at least $1200 \text{ mm} \times 200 \text{ mm}$ area. Scatter plot for time of flight between TOF1 and TOF2, and energy deposit in TOF1 for $0.69\text{-}0.73 \text{ GeV}/c \pi^+, \text{K}^+$ and p are given in Fig. 3-9. Central values of TOF for π^+, K^+ and p are respectively $3.39, 4.09$ and 5.66 ns . The momentum acceptances of them make their widths as $0.11, 0.11$ and 0.19 ns (rms).

Assuming a standard resolution of 0.15 ns for TOF counters, more than 3.7σ separation of K^+ from π^+ and p is possible. GENAT4 simulation shows a conventional counter technique can separate them clearly.

At the trigger level of the experiment, aerogel Cherenkov counters are used for pion rejection and lucite Cherenkov counters will separate kaons from protons.

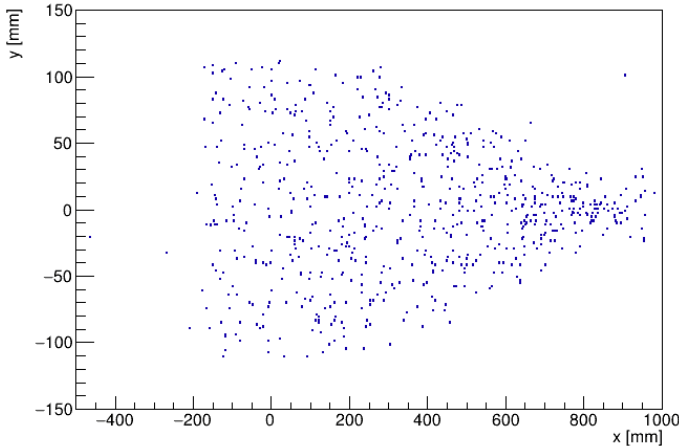


Figure 3-8: Hit position distribution at the front TOF wall.

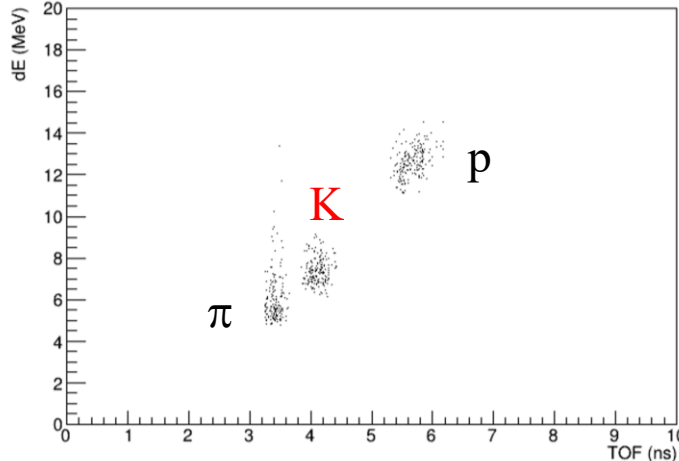


Figure 3-9: Time of flight between two TOF counters vs. energy deposit in TOF1nt TOF wall.

The horizontal beam image $f(x)$ is expressed by the convolution of the horizontal primary beam distribution assumed as a gaussian on the target and a flat distribution with a target image length ($T \cos \theta_{ex}$). Here, θ_{ex} is a beam extraction angle.

$$f(x) = \int_{(-T \sin \theta_{ex})/2}^{(T \sin \theta_{ex})/2} \exp\left(-\frac{(x-u)^2}{2(x_{ptarg})^2}\right) \cos \theta_{ex} du.$$

Let us calculate root mean square of $f(x)$ assuming a platinum target of 60 mm length ($T = 60$ mm) of which material thickness is equivalent to it of 66 mm gold.

Figure 4-2 shows the θ_{ex} dependence of root mean square of horizontal beam image distribution $f(x)$. Though smaller extraction angle (θ_{ex}) and beam size (x_{ptarg}) on the target are favored in terms of beam image size which affects directly the energy resolution of hypernuclear spectroscopy, careful optimization is necessary to have a reasonable π^+ yield, beam spot size and not to disturb other beamlines in the extended hadron hall.

It should be noted that vertical beam image size is almost independent of target length and beam extraction angle.

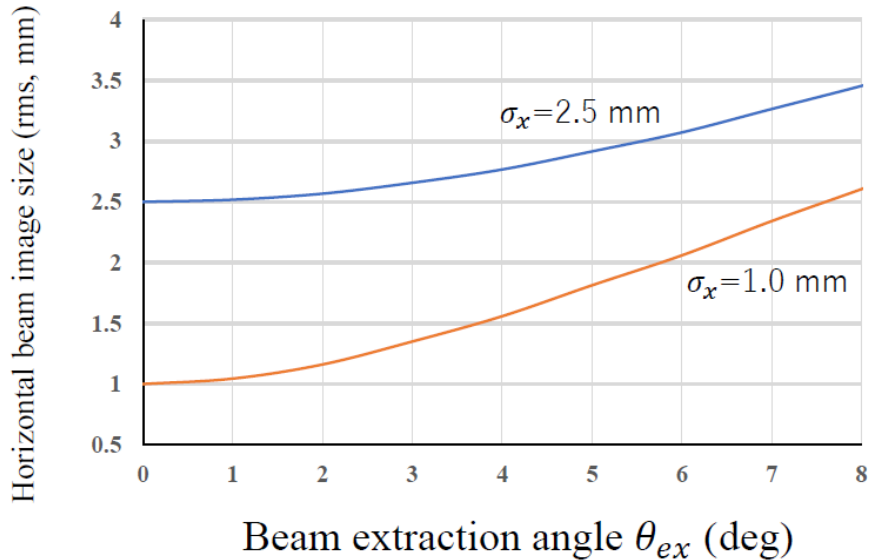


Figure 4-2: Beam extraction angle (θ_{ex}) dependence of horizontal beam image size. Energy resolution of HIHR is highly affected by horizontal beam image size but not by vertical one. Platinum target of 60 mm length is assumed as the primary target. Blue line is for the same beam spot size on existing T1 target ($\sigma_x=2.5$ mm, $\sigma_y = 1$ mm) and orange line is for ($\sigma_x= 1.0$ mm, $\sigma_y = 2.5$ mm) option.

Figure 4-3 shows expected beam intensities in the case that a 30-GeV, 50-kW primary proton beam is irradiated on a 60-mm thick platinum target. About 2.5×10^8 positive pions per beam spill for 1.1 GeV/c π^+ with the beam extraction angle of $\theta_{ex} = 6$ degrees.

Figure 4-4 shows the extraction angle dependence of π^+ intensity. The beam extraction angle should be optimized in a range of 3-6 degrees taking other beam lines conditions into account. For now, extraction angle of 3 degrees for 50 kW primary beam and π^+ intensity of $2 \times 10^8 \pi^+$ /spill at the experimental target are assumed for following hypernuclear yield estimation. It should be noted that no rate limitation exists for detector system of HIHR and beam with a higher pion rate is desirable if future improvement of accelerator makes it possible.

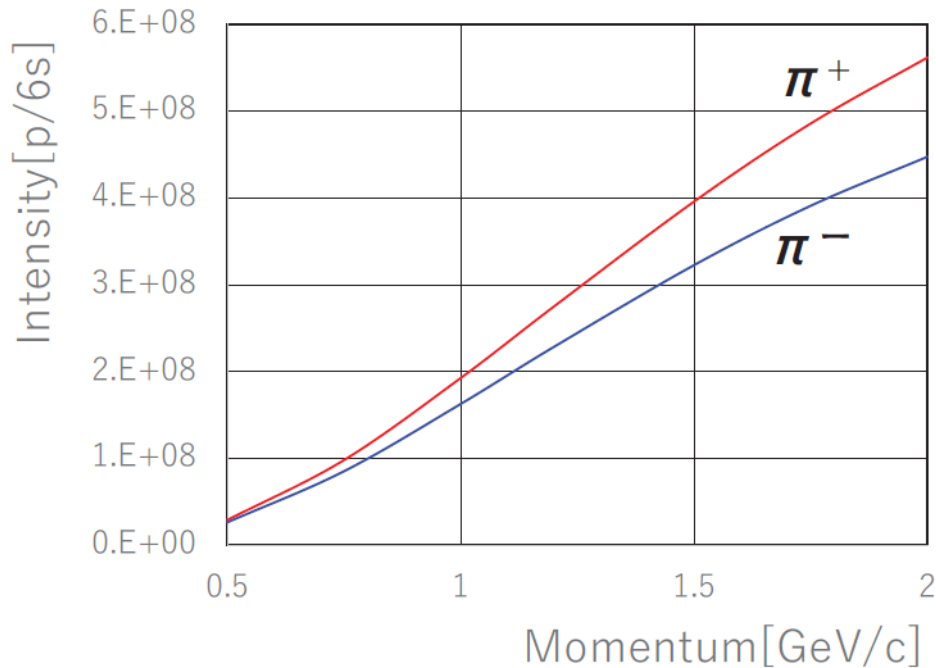


Figure 4-3: Expected beam intensity as a function of beam momentum for 30-GeV, 50-kW primary proton beam is irradiated on a 60-mm thick platinum target and pion beam is extracted with an angle of 6 degrees. The calculation was performed with the Sanford-Wang formula [SAN60]. .

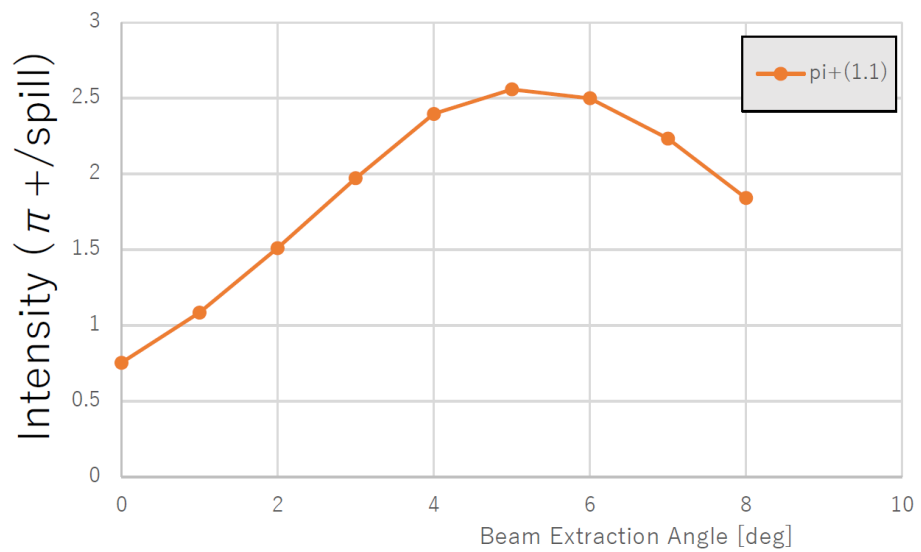


Figure 4-4: Expected beam intensity as a function of beam extraction angle for 30-GeV, 50-kW primary proton beam is irradiated on a 60-mm thick platinum target, calculated by using the Sanford-Wang formula [SAN60].

4.2 Solid angle estimation of kaon spectrometer

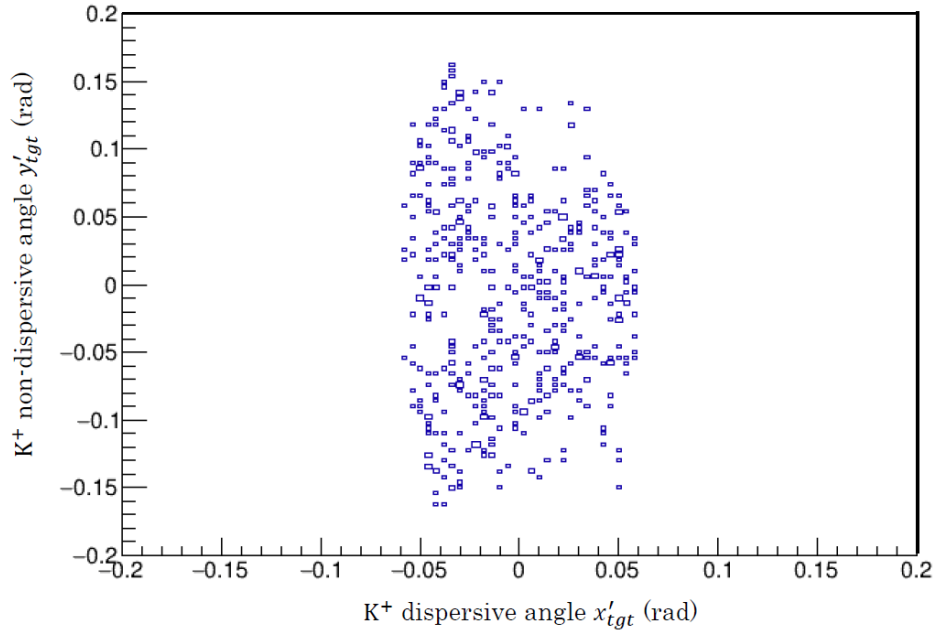


Figure 4-5: Angle distribution of K^+ with a momentum of $0.725 \text{ GeV}/c$ at the experimental target. Events are selected for the particles reached to the focal plane. x'_{tgt} and y'_{tgt} are dispersive and non-dispersive angles.

Solid angle of the kaon spectrometer of HIHR was estimated based on GEANT4 Monte Carlo simulation. Effective width and gap of dipole magnets (D1S, D2S) of the kaon spectrometer were assumed as $100 \text{ cm} \times 20 \text{ cm}$, respectively.

Figure 4-5 shows angular distribution of $0.725 \text{ GeV}/c$ K^+ s passed through the kaon spectrometer. Solid angle of the spectrometer was estimated as $\Omega = 4\pi N_{fp}/N_{gen}$, where N_{fp} is the number of K^+ s which reach to the focal plane and N_{gen} is the number of uniformly generated K^+ s in the simulation.

Figure 4-6 shows momentum dependence of the solid angles of the kaon spectrometer with and without vertical angular selection at the experimental target. There would be a room for optimization, but resolution for the events with larger $|y'_{target}|$ tends to be worse. Therefore $|y'_{target}| < 0.1 \text{ rad}$ is now assumed to make the solid angle flat over kaon momentum acceptance. Applying this cut, solid angle is about 20 msr over entire momentum acceptance.

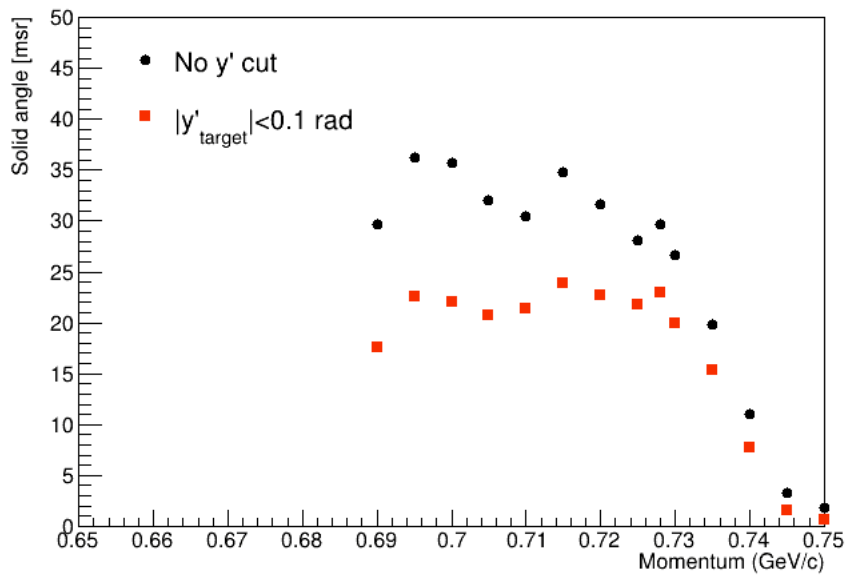


Figure 4-6: Solid angle of the kaon spectrometer as a function of kaon momentum. Red dots show the solid angle with a selection of $|y'_{target}| < 0.1$ rad and block ones without the selection. On the experimental target, uniform distribution of reaction points for $|x_{target}| < 50$ mm was assumed for this simulation.

4.3 Yield estimation of ${}^{12}_{\Lambda}\text{C}$

Reaction spectroscopy of Λ hypernuclei normally utilize a carbon target as a reference and commissioning of setup because easy handling of solid target and nuclear structure of ${}^{12}_{\Lambda}\text{C}$ has been well studied.

It is assumed that primary proton of 30 GeV, 50 kW bombarded the target of platinum 60 mm length with a beam spot size of $2.5 \times 1.0 \text{ mm}^2$. Beam repetition cycle The meson extraction angle of 3 degrees was assumed. The experimental target of ${}^{12}\text{C}$ of 400 mg/cm^2 is assumed to achieve about 400 keV energy resolution as discussed in the next section.

Cross section of ${}^{12}\text{C}(\pi^+, K^+){}^{12}_{\Lambda}\text{C}$ is assumed as $8.1 \mu\text{b/sr}$ which is an average of 2-14 degrees for kaon emission angles [HOT01]. In the proposed experiment, kaon emission angle of 0 degrees will be measured and thus cross section is expected to be slightly larger than the assumed value. Key parameters for ${}^{12}_{\Lambda}\text{C}$ yield estimation are summarized in Table 4-I.

Table 4-I: Hypernuclear yield estimation for ${}^{12}_{\Lambda}\text{C}$ at HIHR.

| | HIHR@J-PARC |
|--|--|
| Primary proton beam | 30 GeV, 50 kW repetition cycle 5.2 s |
| Central momentum of π^+ beam | 1.1 GeV/c |
| π^+ beam rate at IF2 | $3.85 \times 10^7/\text{sec}$ (200 M π^+ /spill) |
| ${}^{12}\text{C}$ target thickness | 400 mg/cm^2 ($1.8 \text{ g/cm}^3 \times 0.22 \text{ cm}$) |
| Reaction | ${}^{12}\text{C}(\pi^+, K^+){}^{12}_{\Lambda}\text{C}$ |
| Cross section of ground state of ${}^{12}_{\Lambda}\text{C}$ | $8.1 \mu\text{b/sr}$ |
| Central momentum of K^+ | 0.71 GeV/c |
| Solid angle of kaon spectrometer | >20 msr |
| Kaon survival ratio | 0.12 11.4 m for QSQDMD |
| Estimated count rate of ${}^{12}_{\Lambda}\text{C}_{gs}$ | 53.1 counts/hr |

5. Resolution estimation

Detailed design of HIHR and target will be optimized in collaboration with J-PARC beamline group. The energy resolution estimation was carried out with an optics code TRANSPORT and Monte Carlo package GEANT4.

5.1 TRANSPORT, optics code study

The following factors contribute to the total energy resolution of the (π^+ , K^+) reaction spectroscopy experiment.

1. Beam momentum resolution.

Though a separate discussion of beam momentum resolution is not necessary to evaluate the total energy resolution of Λ hypernuclei for a dispersion matching experiment, the beam momentum resolution plays an important role in calibration as well as a possible option of non-dispersion matching experiment. Therefore, it is useful to estimate beam momentum resolution based on the first order beam optics. Assuming beam image size at IF2 as $\sigma_x = 1$ mm, magnification ($x_{tgt}|x_0$)=1.3 and dispersion ($x_{tgt}|\delta$)=11.28 cm/%, momentum resolution is estimated as $dp/p = 2.4 \times 10^{-4}$ for a 1.1 GeV/c π^+ beam. It corresponds to 250 keV/c (FWHM).

2. Kaon spectrometer momentum resolution.

Similar to the beam momentum resolution, separate discussion of kaon spectrometer is not necessary to estimate the total energy resolution of HIHR. Position resolution of 0.2 mm (rms) and tracking efficiency of 99.8% is assumed as they are achieved for SKS tracking chamber at K1.8 beamline of J-PARC [TAK12]. Dispersion ($x_{fp}|\delta$)=10.72 cm/% and a point source are assumed, momentum resolution of $dp/p = 1.9 \times 10^{-4}$ for a 0.71 GeV/c K^+ beam. It corresponds to 32 keV/c (FWHM). Beam size on the target will contribute in addition to this value. With magnification of ($x_{fp}|x_{tgt}$)=1.84 and reaction point uncertainty of 1.3 mm, momentum resolution including this contribution is estimated as 370 keV/c (FWHM).

Momentum dispersion match operation needs a thin solid target but additional tracking device after the target will make it possible to optically separate beam and kaon spectrometers for non-dispersion matching operation. It should be noted that high resolution (sub-MeV) spectroscopy is also possible for a thick gaseous target with this non-dispersion matching operation of HIHR at the cost of maximum π^+ intensity.

3. Energy loss and straggling in the target.

Since we have no information of reaction point in a solid target (typically the thickness of the target is less than a millimeter for a material thickness of 100-400 mg/cm²), energy loss of charged particles can be corrected only as an average. Its distribution including straggling will contribute the final mass resolution. Most probable energy loss (Δ_p) and straggling (w) were calculated with Landau-Vavilov formula and compiled in Tab. 5-I. Angular distribution affects the effective thickness of the target, however, horizontal angular acceptance of the kaon spectrometer is ± 50 mr and this effect is estimated as $|\{1/\cos(5 \times 10^{-2})\} - 1| \approx 1.3 \times 10^{-3}$ which can be safely neglected.

With the above estimation into account, the second order ion optics calculation with TRANSPORT was performed.

Table 5-I: Most probable energy loss and straggling for typical solid targets with a thickness of 50/100/200 mg/cm². They correspond to the cases for reaction at the center of 100/200/400 mg/cm² thick target. Unit is keV.

| Target | Thickness (mg/cm ²) | 1.1 GeV/c π^+ | | 0.71 GeV/c K^+ | |
|-------------------|------------------------------------|-------------------|----------|------------------|----------|
| | | Δ_p (MPV) | w (FWHM) | Δ_p (MPV) | w (FWHM) |
| ¹⁰ B | 200 | 136 | 31 | 124 | 36 |
| ¹² C | 100 | 65 | 16 | 59 | 18 |
| ¹² C | 200 | 136 | 31 | 124 | 36 |
| ¹² C | 400 | 283 | 62 | 260 | 72 |
| ²⁸ Si | 400 | 258 | 62 | 232 | 72 |
| ⁵¹ V | 400 | 221 | 56 | 196 | 65 |
| ⁸⁹ Y | 400 | 203 | 55 | 176 | 63 |
| ¹³⁹ La | 400 | 182 | 51 | 156 | 59 |
| ²⁰⁸ Pb | 400 | 162 | 49 | 135 | 57 |

Figure 5-1 shows horizontal position distribution of K^+ s emitted at the focal plane calculated by the second order optical calculation. Kaon emission angle at the experimental target was assumed as $\theta_K = 0$ and energy loss and straggling effects in the target were not included in this calculation. Therefore, this result reflects purely beamline and spectrometer optical features. The first peak corresponds to the ground state of $^{12}_\Lambda C$ and the second peak is an artificially created excited state with $E_x = 5$ MeV. Peak width was fitted as $\sigma = 0.161$ cm and it can be converted to the energy resolution (optics) as:

$$\Delta E_{opt} = 2\sqrt{2 \ln 2} \times 0.161 \text{ cm} \times \frac{5 \text{ MeV}}{6.02 \text{ cm}} = 315 \text{ keV (FWHM)}.$$

This resolution shows ideally achievable value for a very thin target with complete dispersion matching conditions are satisfied.

Let us summarize results of energy resolution studies with the optics code TRANSPORT in Table 5-II.

Taking energy loss and straggling effects into account, energy resolution is estimated as better than 0.4 MeV for the ground state of $^{12}_\Lambda C$.

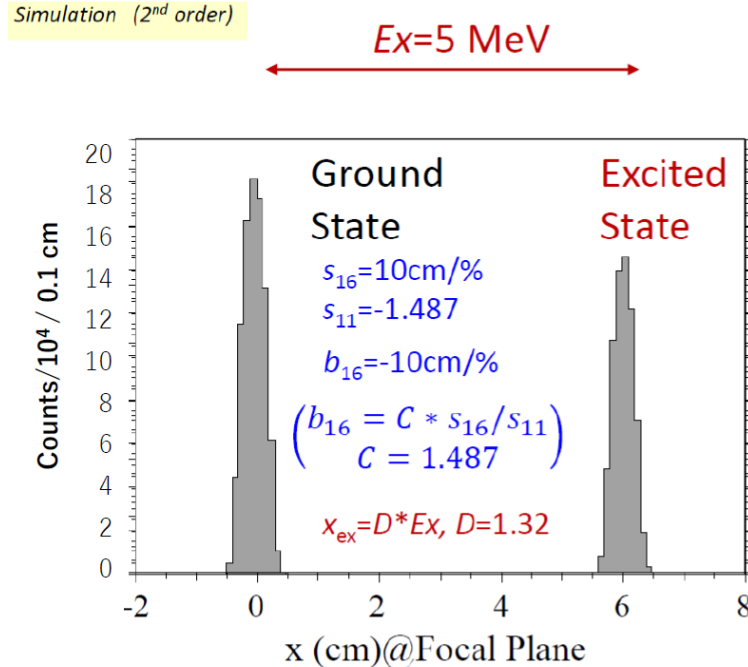


Figure 5-1: Horizontal position distribution at the focal plane calculated by the second order optical calculation.

Table 5-II: Summary of energy resolution study with TRANSPORT

| | TRANSPORT Optical code |
|---|--|
| Reaction | $^{12}\text{C}(\pi^+, K^+)^{12}_{\Lambda}\text{C}$ |
| π^+ beamline momentum resolution (FWHM) | 0.25 MeV/c |
| K^+ spectrometer momentum resolution (FWHM) | 0.37 MeV/c |
| Energy resolution of beam optics (FWHM) | 0.32 MeV |
| Energy loss and straggling in target (100mg/cm ² $^{12}_{\Lambda}\text{C}$) | 0.09 MeV |
| Mass resolution of $^{12}_{\Lambda}\text{C}$ (FWHM) | 0.33 MeV |

5.2 GEANT4, Monte Carlo simulation study

As shown in Fig. 3-4, the HIHR dispersion matching beam line after IF2, an experimental target and the kaon spectrometer were modeled in GEANT4 simulation code. Optics code is useful for quick optimization of magnet parameters, and it is suitable to examine the rough behavior of the system. On the contrary, Monte Carlo simulation takes longer time and tunes of beam element parameters are not straightforward as the optics code does, but it is necessary to investigate the behavior of a complex system in which various factors are intertwined.

Ideal magnetic fields for dipole, quadrupole and sextupole magnets were now assumed in the model and they should be replaced by more realistic fields map calculated by 3D finite element method such as TOSCA or measured magnetic field after detailed design or fabrication of magnets.

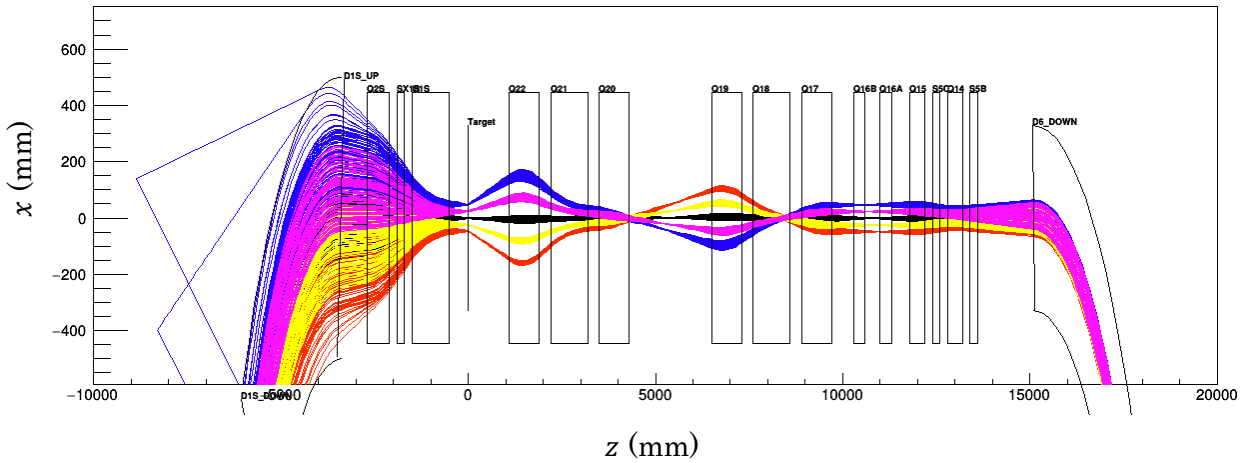


Figure 5-2: Example of beam trajectories simulated by GEANT4. Beam color (red, yellow, black, magenta and blue) corresponds to π^+ beam momenta of 1.045, 1.0475, 1.050, 1.0525 and 1.055 GeV/c, respectively.

Figure 5-2 shows GEANT4 simulated beam trajectories. It can be seen that momentum spread of beam π^+ was converted to spatial distribution at the experimental target ($z = 0$) as expected.

In the simulation, following processes were taken into account. Passing through the experimental target, beam π^+ loses its energy, experiences multiple scattering and finally react with a target nucleus through the $^{12}\text{C}(\pi^+, K^+)^{12}\text{C}$ reaction. In this section, excitation

energies of 0, 5, 10, 15 MeV were considered (they are nothing to do with real ^{12}C structure) and K^+ emission angles were uniformly distributed in the angular acceptance.

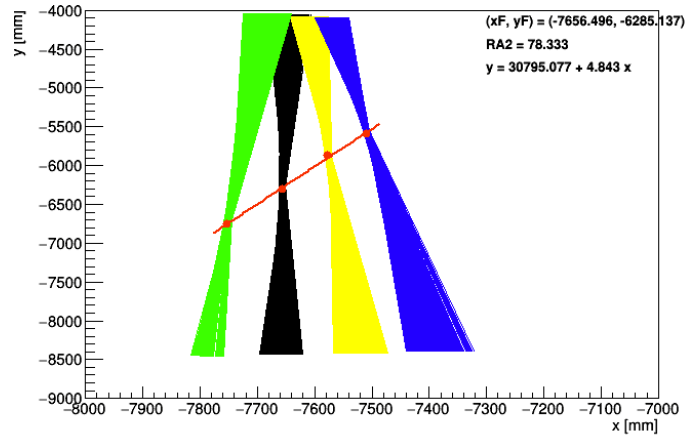


Figure 5-3: Example of K^+ trajectories simulated by GEANT4. Beam color (green, black yellow and blue) corresponds to the excitation energy of 15, 10, 5, 0 MeV for $^{12}\text{C}(\pi^+, \text{K}^+)^{12}\text{C}$ reaction. Measurement of beam position gives excitation energy.

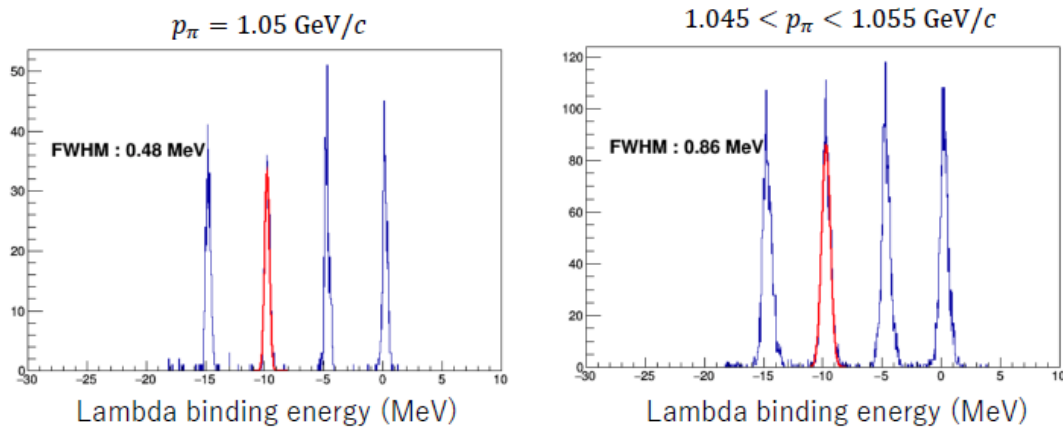


Figure 5-4: Lambda binding energy spectrum for $p_\pi = 1.05 \text{ GeV}/c$ (left) and $1.045 < p_\pi < 1.055 \text{ GeV}/c$ (right).

Figure 5-3 shows that K^+ s with the same excitation energy converge at the focal plane and it is different from the case that K^+ s with the same momentum from a point source converge at the focal plane of a normal spectrometer.

The K^+ horizontal position distribution was converted to Lambda binding energy (B_Λ). Figure 5-4 (left) shows $-B_\Lambda$ for beam pion momentum was selected as $p_\pi = 1.05$ GeV/c, and (right) shows it for $1.045 < p_\pi < 1.055$ GeV/c. Energy resolution for $p_\pi = 1.05$ GeV/c, was 0.48 MeV (FWHM) and it for $1.045 < p_\pi < 1.055$ GeV/c was 0.86 MeV (FWHM). It is known that deterioration of energy resolution in this simulation was caused by an imperfect alignment of focal planes for different beam momenta. Ideally intrinsic resolution of HIHR beam optics system is expected to approach the ideal value, 315 keV (FWHM) as shown by TRANSPORT calculation in the previous section. Further GEANT4 simulation study on beam elements tunes with higher order optical elements for better dispersion matching condition is in progress.

It should be noted that the resolution was discussed here assuming use of the kaon spectrometer as a “hardware spectrometer” which has a clean focal plane and gives energy or momentum information as a dispersive position information. Recent progresses of computer power enable us to obtain resolution of $\Delta p/p = 2 \times 10^{-4}$ for a so-called “software spectrometer”, which has no clear focal plane, by using 6 orders polynomial function of position and angle information of x, x', y, y' at reference plane [GOG18]. Introduction of such techniques would enable us to compensate higher order aberration which cannot be compensated perfectly by hardware and contribute to improve energy resolution.

By using GEANT4 simulation, how target thickness affects energy resolution was studied. Target thickness affects energy resolution in following two ways and these effects are automatically included in the result of GEANT4 simulation.

- 1) Effective thickness changes due to K^+ emission angle. This effect is already discussed in the previous section. and it is safely neglected.
- 2) Energy loss depends on the reaction position. If the reaction happens near to front surface of the target, $p(\pi^+)$ is larger than it is expected for the case the reaction happens at the center of the target, since energy loss in the target is smaller.

The same thing happens for emitted K^+ . If the reaction happens near to front, actual $p(K^+)$ is also larger than it measured by the kaon spectrometer. If reaction happens near to back surface of the target, the opposite effects will be observed. In addition to energy loss effects, energy straggling occurs even if the reaction point does not move.

These effects can be easily estimated with GEANT4 simulation. Preparing relatively thick target in the model and reaction points were uniformly distributed along the incoming beam direction, then spatial distribution of K^+ s at the focal plane was measured and converted to the energy scale. This study shows that 1 mm change of reaction point along the beam direction in the ^{12}C target corresponds to 78.5 keV change of missing mass of ^{12}C . Since 200 mg/cm^2 of ^{12}C (density 1.8 g/cm^3) is 1.1 mm thick, energy loss and straggling give 87.2 keV deterioration to the energy resolution.

Final result of target thickness dependence of energy resolution for ^{12}C (density 1.8 g/cm^3) with $p_\pi = 1.05 \text{ GeV}/c$ was shown in Fig. 5-5. Black points show the resolution for all generated events and red points for the events with K^+ angular acceptance cuts of $|x'_{target}| < 20 \text{ mr}$ and $|y'_{target}| < 20 \text{ mr}$. Red points give better resolution because momentum matching conditions are less satisfied for the events with larger emission angles. It indicates that further study of optics tuning is essentially important as well as limitation of angular acceptance results in improvement of resolution (250 keV (FWHM) for the thin target limit) at the cost of yield.

Looking black points, it can be seen that up to 400 mg/cm^2 which corresponds to 2 mm-thick ^{12}C , intrinsic resolution of optics system dominates under currently achieved matching condition. For target thickness over 400 mg/cm^2 energy straggling and other factors in target begin to contribute to the energy resolution. Limitation of K^+ angular acceptance makes intrinsic optical resolution good enough to see almost pure target thickness dependence as shown by red points.

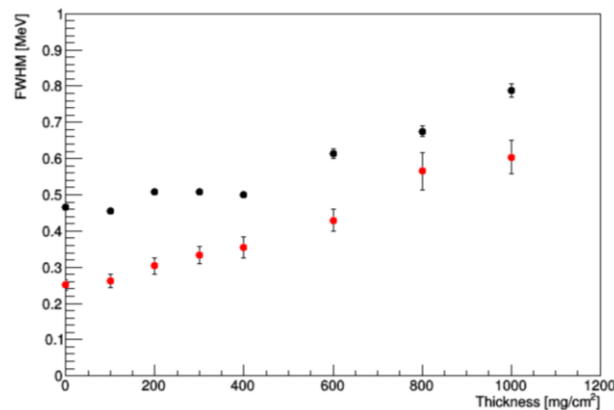


Figure 5-5: Target thickness dependence of the energy resolution for ^{12}C target. Black points and red points are respectively without and with angular acceptance selection of $|x'_{target}| < 20 \text{ mr}$ and $|y'_{target}| < 20 \text{ mr}$.

5.3 Summary of energy resolution study

The energy resolution estimation was carried out with an optics code TRANSPORT and a Monte Carlo package GEANT4. Optics code has advantages of quick matrix tuning and easier investigation of optical features of the beamline and spectrometer systems. However, detailed study with reactions in the target cannot be carried out. On the contrary to the optics code, Monte Carlo simulation can easily consider various reactions in materials on the beamline but tuning of beam elements is not easy as the optics code. During conceptual design works, both optics code and simulation studies will be complementarily performed.

When a reliable design of magnets is finalized and detailed magnetic field maps are implemented in the simulation code, a thorough optimization of optical parameters will be performed. After such an optimization, adjustments for minor change of experimental condition will be quickly done with a dedicated GEANT4 simulation code to be developed for this purpose.

Though further study and optimization of beamline components are necessary, current study shows that the dispersion match technique enables an energy resolution of better than 400 keV (FWHM) for less than 400 mg/cm² targets at HIHR. Limitation of acceptance with a thin target might enable further improvement of the resolution at the cost of hypernuclear yield. Target thickness and acceptance limitation will be optimized depending on the experimental requirements, such as resolution or yield.

Figure 5-6 shows expected Λ binding energy spectra for $^{12}_{\Lambda}\text{C}$ (left) and $^{208}_{\Lambda}\text{Pb}$ (right). They should be compared with previously measured spectra at KEK (Fig. 5-7).

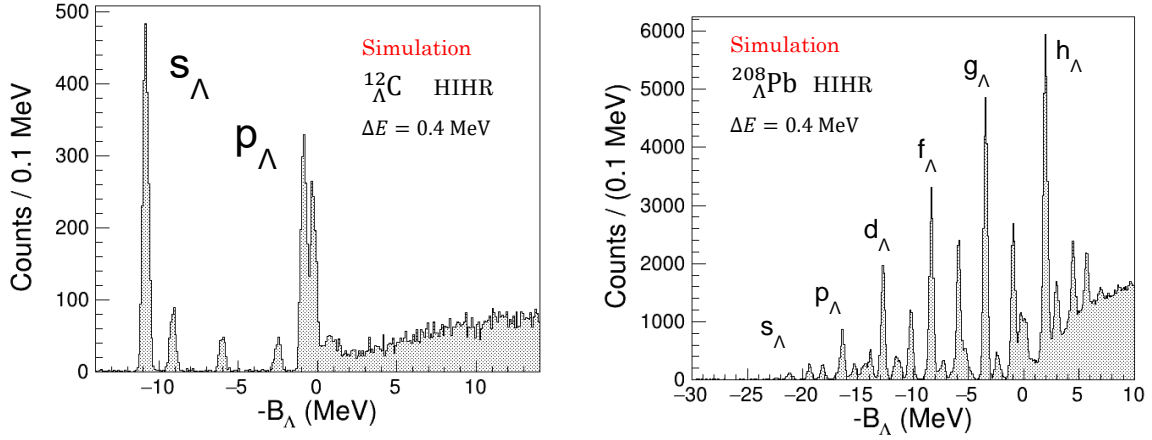


Figure 5-6: Expected Λ binding energy spectra for $^{12}_{\Lambda}\text{C}$ (left) and $^{208}_{\Lambda}\text{Pb}$ (right). Resolution of 0.4 MeV (FWHM) and number of the events for the ground states of 1000 and 100 were assumed for $^{12}_{\Lambda}\text{C}$ and $^{208}_{\Lambda}\text{Pb}$, respectively as requested in section 6.

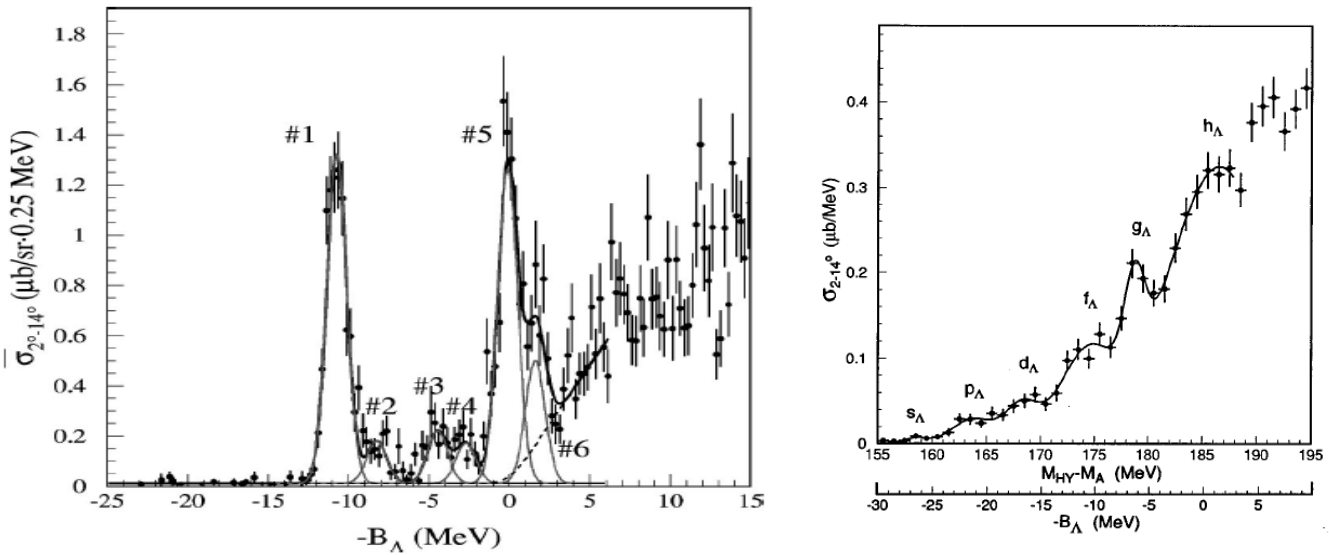


Figure 5-7: Previously measured Λ binding energy spectra for $^{12}_{\Lambda}\text{C}$ (left) [HOT01] and $^{208}_{\Lambda}\text{Pb}$ (right) [HAS]. Resolutions were 1.45 MeV (FWHM) and 2.3 MeV (FWHM) for $^{12}_{\Lambda}\text{C}$ and $^{208}_{\Lambda}\text{Pb}$, respectively.

6. Beamtime request

The targets listed in Table 6-I are required to achieve the original goal of this proposal, but choice of targets is not limited, because HIHR aims to be the *hypernuclear factory* for wide variety of experiments.

Since HIHR is a brand-new beamline, commission time for hardware development will be requested separately.

Assuming the energy resolution of HIHR is 400 keV (FWHM) as discussed in section 5, more than 100 events of a peak can determine the peak centroid with a statistical error better than $400\text{keV} / \sqrt{100} \approx 40$ keV. Typically, cross sections of excited bound states of Λ binding energy of heavy hypernuclei are several times larger than they for the ground states, for example, cross sections of Λ in s -orbit (ground state) and p -orbit $^{208}\text{Pb}(\pi^+, K^+) ^{208}_{\Lambda}\text{Pb}$ are respectively 0.2 and 0.8 $\mu\text{b}/\text{sr}$. Therefore, statistical uncertainty of binding energies for excited bound states would be a few 10 keV.

Background shape ambiguity, accuracy of energy scale calibration would contribute to systematic errors, but overall uncertainties of binding energies of hypernuclei can be controlled to be less than 100 keV.

Carbon target is normally used as a reference for reaction spectroscopy of hypernuclei. Optimized parameters of magnetic elements for dispersion matching condition will be investigated with the carbon runs. During beamline tuning, limitation of acceptance will be applied to have clean events with the best energy resolution which is optically achievable and thus higher statistics is essentially important. Reference data for various target thickness (100, 200, 400 mg/cm^2) will be accumulated.

It should be noted that (π^+, K^+) reaction hypernuclear spectroscopy cannot use hyperon (Λ and Σ^0) masses as the absolute mass calibration sources due to unavailability of neutron target, and thus $^{12}_{\Lambda}\text{C}$ mass will serve as one of energy references. All previous (π^+, K^+) experiments used the $^{12}_{\Lambda}\text{C}$ mass as the mass calibration, but it was pointed out that old $^{12}_{\Lambda}\text{C}$ mass measured by nuclear emulsion almost half a century ago would have a large error [GOG16, BOT17]. Recent state-of-art hybrid emulsion experiment, J-PARC E07, has lots of $^{12}_{\Lambda}\text{C}$ events and analysis of these events will provide a new $^{12}_{\Lambda}\text{C}$ mass reference in near future. Decay pion spectroscopic experiment at HIHR is now planned [FUJ21, NAG18] and it will serve as an independent calibration source.

For light to medium heavy targets, hypernuclear production cross section for ground state is relatively large and thus beamtime for 100 events accumulations with 200 mg/cm² thick targets are requested.

For heavy targets, cross sections of ground states are small and energy level density is large. Therefore luminosity-oriented beamtime to measure ground state which needs high statistics and resolution-oriented beamtime to separate complicate excitation energy levels which have larger cross sections than the ground state, are separately requested.

Beamtimes for light to medium-heavy hypernuclei need 724 hours (30 days) and heavy targets need 1764 hours (73 days), ground total of 2488 hours (104 days) for the first campaign of experiments at HIHR. Divided beamtime allocation is desirable rather than a continuous one, because time for analysis of accumulated data is important to feed back its result to the next beamtime.

Table 6-I : Summary of requesting beamtime for 50 kW proton beam power. Differential cross sections at $\theta_K \sim 0$ were estimated by using data of prior (π^+ , K^+) experiments [PIL91, HAS94, HAS96, HOT01, HAS06].

| | Assumed g.s. Cross Section ($\mu\text{b/sr}$) | Target thickness (mg/cm^2) | Expected Yield(/h) | Requested number of events for g.s. | Beam Time (h) |
|---|---|---|-------------------------------|--|--------------------------|
| $^{12}_{\Lambda}\text{C}$ | 8.1 | 100 | 13.3 | 1000 | 79 |
| $^{12}_{\Lambda}\text{C}$ | 8.1 | 200 | 26.6 | 2000 | 79 |
| $^{12}_{\Lambda}\text{C}$ | 8.1 | 400 | 53.1 | 2000 | 39 |
| $^6_{\Lambda}\text{Li}$ | 1.9 | 200 | 12.7 | 100 | 8 |
| $^7_{\Lambda}\text{Li}$ | 1.9 | 200 | 10.9 | 100 | 10 |
| $^9_{\Lambda}\text{Be}$ | 0.2 | 200 | 1.1 | 100 | 98 |
| $^{10}_{\Lambda}\text{B}$ | 0.9 | 200 | 3.5 | 100 | 30 |
| $^{11}_{\Lambda}\text{B}$ | 0.9 | 200 | 3.2 | 100 | 33 |
| $^{28}_{\Lambda}\text{Si}$ | 0.5 | 400 | 1.4 | 100 | 75 |
| $^{40}_{\Lambda}\text{Ca}$ | 0.5 | 400 | 0.94 | 100 | 112 |
| $^{51}_{\Lambda}\text{V}$ | 1.2 | 400 | 1.8 | 100 | 59 |
| $^{89}_{\Lambda}\text{Y}$ | 0.6 | 400 | 0.53 | 100 | 199 |
| Sub total (light- mid heavy) | | | | | 724 (30 days) |

| | | | | | |
|-----------------------------|------------|------------|--------------|-----------|---------------------------|
| $^{139}_{\Lambda}\text{La}$ | 0.3 | 200 | 0.085 | 20 | 236 |
| $^{139}_{\Lambda}\text{La}$ | 0.3 | 400 | 0.17 | 80 | 471 |
| $^{208}_{\Lambda}\text{Pb}$ | 0.3 | 200 | 0.057 | 20 | 352 |
| $^{208}_{\Lambda}\text{Pb}$ | 0.3 | 400 | 0.11 | 80 | 705 |
| Sub total (heavy) | | | | | 1764 (73 days) |
| Grand Total | | | | | 2488 (104 days) |

7. Summary

Based on a newly designed momentum matching pion beamline with a specially designed kaon spectrometer system, HIHR at the J-PARC hadron extension hall, a campaign of Λ hypernuclear (π^+ , K^+) reaction spectroscopy experiments was proposed.

Unprecedented energy resolution of <400 keV (FWHM) as a hypernuclear reaction spectroscopy with high statistics >100 events for ground states of various Λ hypernuclei will enable us to determine Λ binding energies with an accuracy better than 100 keV. Precise determination of hypernuclear binding energies in wide mass region enables us to clarify the existence of the Λ NN three-body repulsive force which is a key to solve the puzzle of heavy neutron stars (hyperon puzzle). HIHR will be a unique hypernuclear factory which provides various high precision data to construct a reliable baryonic interaction model and such experiments cannot be performed at other facilities.

Key Experimental Parameters:

| | |
|---------------------------------------|---|
| Primary beam energy: | 30 GeV |
| Primary beam intensity: | > 50 kW |
| Beam spot size on the primary target: | $\sigma_x < 1$ mm |
| Beam extraction angle: | 3 degrees |
| Secondary beam: | 1.05 GeV/c π^+ |
| Beamline & Spectrometer: | HIHR |
| Targets: | ^{12}C , $^{6,7}\text{Li}$, ^9Be , $^{10,11}\text{B}$, ^{28}Si , ^{40}Ca , ^{51}V , ^{89}Y ^{139}La , ^{208}Pb |

Requested beam time:

Light targets : 724 h = 30 days for light targets

Heavy targets : 1764 h = 73 days for heavy targets

Grand total: 2488 h = 104 days for 50 kW beam

Separate beamtimes for commission of hardware are necessary.

References

- [AGA12] K.Agari et al., Prog.Theor. Exp. Phys. (2012) 02B009.
- [AMB60] V. A. Ambartsumyan and G. S. Saakyan, Sov. Astron. AJ 4, 187 (1960).
- [ANT13] J. Antoniadis, N. Gargueron, and G. Chanfray, Europhys. Lett. 97, 39002 (2012).
- [AOK10] S.Aoki, T.Hatsuda, N.Ishii PTP 123 (2010) 89.
- [AOK11] S.Aoki et al., Proc. Jpn. Acad. B87 (2011) 509.
- [BED12] I. Bednarek, et al., Astron. Astrophys. 543, A157 (2012).
- [BOD84] A. R. Bodmer, Q. N. Usmani, and J. Carlson, Phys. Rev. C 29, 684 (1984); A. R. Bodmer and Q. N. Usmani, Phys. Rev. C 31, 1400 (1985).; A. R. Bodmer and Q. N. Usmani, Nucl. Phys. A 477, 621 (1988).
- [BOM16] I.Bombaci, ArXiv:1601.05339; to be published as HYP2015 Proceedings.
- [BOT17] E.Botta et al., Nucl. Phys. A 960 (2017) 165.
- [BUR21] G.F.Burgio, H.-J.Schulze, I. Vidaña, j.-B. Wei, ArXiv:2015.03747.
- [CHA16] D.Chatterjee and Isaac Vidaña, Eur. Phys. J. A (2016)52:29.
- [CRO20] H.T.Cromartie, et al., Nature Astronomy 4, (2020) 72.
- [DAV92] D.H. Davis, Nucl. Phys. A547 (1992) 369c.
- [DEM10] P. B. Demorest, et al., Nature 467, 1081 (2010).
- [DOV87] C.B. Dover, Proc. Int. Symp. on Medium Energy Physics, Beijing, World Scientific, Singapore, (1987) 257.
- [EKS13] A. Ekstrom et al., Phys. Rev. Lett. 110, 192502 (2013).
- [EPE05] E. Epelbaum, W. Glockle, and Ulf-G. Meissner, Nucl. Phys. A 747, 0375 (2005).
- [ESS15] A.Esser, S.Nagao, F.Schulz et al., Phys. Rev. Lett. 114 (2015) 232501.
- [EUR16] EurekAlert! “New spectroscopy of Be¹⁰L hypernucleus redefines the reference data of Lambda hypernuclei”, http://www.eurekalert.org/pub_releases/2016-04/tunso040616.php
- [FRO87] B. Frois and C. N. Papanicolas, Ann. Rev. Nucl. Part. Sci. 37, 133 (1987).
- [FUJ21] H.Fujioka, HIHR/K1.1 workshop, May 23, 2021.
- [FUJ97] Y.Fujita et al., Nucl. Inst. and Meth. B 126 (1997) 274.
- [FUJ99] M.Fujiwara et al., Nucl. Inst. and Meth. A 422 (1999) 484.
- [FUK95] T. Fukuda et al., Nucl. Inst. and Meth. A 361 (1995) 485.
- [FUR09] T. Furumoto, Y. Sakuragi, Y. Yamamoto, Phys. Rev. C 79 (2009) 0011601(R).
- [GAL16] A.Gal, E.V. Hungerford, D.J. Millener, Rev. Mod. Phys. 88 (2016) 035004.

- [GAN12] S. Gandolfi, J. Carlson, and S. Reddy, Phys. Rev. C 85, 032801 (2012); S. Gandolfi, J. Carlson, S. Reddy, A. W. Steiner, and R. B. Wiringa, Eur. Phys. J. A 50, 10 (2014).
- [GAZ16] D.Gazda and A.Gal, Nucl. Phys. A 954 (2016) 161.
- [GER20] D.Gerstung, N.Kaiser and W.Weise, Eur. Phys. J. A. (2020) 56:175.
- [GEZ13] A. Gezerlis et al., Phys. Rev. Lett. 111, 032501 (2013).
- [GOG16] T.Gogami et al., Phys. Rev. C 93, 034314 (2016).
- [GOG16-2] T.Gogami et al., Phys. Rev. C 94 (2016) 021302(R).
- [GOG18] T.Gogami et al., Nucl. Inst. and Meth. A 900 (2018) 69.
- [GOG21] T.Gogami et al., Phys. Rev. C 103 (2021) L041301.
- [HAI05] J. Haidenbauer and Ulf-G. Meißner, Phys. Rev. C 72 (2005) 044005.
- [HAI07] J.Haidenbauer, U.-G. Meißner, N.Kiser and W.Weise, Eur. Phys. J. A (2017) 53: 121.
- [HAI13] J.Haidenbauer et al., Nucl. Phys. A 915 (2013) 24.
- [HAI20] J.Haidenbauer, U.-G.Meißner, A.Nogga, Eur. Phys. J. A (2020) 56:91.
- [HAI20-2]J. Hadenbauer and I.Vidana, Eur. Phys. J. A (2020) 56:55.
- [HAS06] O.Hashimoto and H.Tamura, Prog. Part. Nucl. Phys. 57 (2006) 564.
- [HAS94] T.Hasegawa, Doctor Thesis (Univ. of Tokyo), INS-IM-15, 1994.
- [HAS95] T. Hasegawa et al. Phys. Rev. Lett. 74 (1995) 224.
- [HAS96] T.Hasegawa et al., Phys. Rev. C 53 (1996) 1210.
- [HAS98] O.Hashimoto et al., Nucl. Phys. A 639 (1998) 93c.
- [HIY01] E.Hiyama et al., PRC 65, 011301(R) (2001)
- [HIY09] E.Hiyama and T.Yamada, Prog. Part. Nucl. Phys. 63 (2009) 339.
- [HOT01]H.Hotch et al., Phys. Rev. C 64 (2001) 044302.
- [IMR14] M. Imran, A. A. Usmani, M. Ikram, Z. Hasan, and F. C. Khanna, J. Phys. G 41, 065101 (2014).
- [ISA13] M. Isaka et al., Phys. Rev. C 87, 021304R (2013)
- [ISA16] M.Isaka, Y.Yamamoto and Th.A.Rijken, Phys. Rev. C 94 (2016) 044310; M.Isaka, Y.Yamamoto and Th.A.Rijken, presentation at JLab Hypernuclear workshop (2016).
- [ISA17] M.Isaka, Y.Yamamoto and Th.A.Rijken, Phys. Rev. C 95 (2017) 044308.
- [ISH12] N.Ishii et al., PLB712 (2012) 437.
- [JUR73] M.Juric, Nucl. Phys. B52 (1973) 1.
- [KAI00] C.M. Keil, F. Hofmann, H.Lenske, Phys. Rev. C 61 (2000) 064309; H. Lenske,

presentation at HYP2006 (2006) Mainz

- [KOH18] M. Kohno, Phys. Rev. C 97 (2018) 035206.
- [LE20] H.Le, J. Haidenbauer, U.-G. Meißner, A.Nogga, Eur. Phys. J. A (2020) 56:301.
- [LER07] JLab Hypernuclear Collaboration, PR12-13-002 submitted to JLab PAC40.
- [LON14] D. Lonardoni, F. Pederiva, and S. Gandolfi, Phys. Rev. C 89, 014314 (2014).
- [LON15] D. Lonardoni, A. Lovato, S. Gandolfi, and F. Pederiva, Phys. Rev. Lett. 114, 092301 (2015).
- [LOP14] L. L. Lopes, and D. P. Menezes, Phys. Rev. C 89, 025805 (2014).
- [MAC96] R. Machleidt, F. Sammarruca, and Y. Song, Phys. Rev. C 53, R1483 (1996).
- [MAR13] P. Maris, J. P. Vary, S. Gandolfi, J. Carlson, and S. C. Pieper, Phys. Rev. C 87, 054318 (2013).
- [MIL85] C. Milner et al., Phys. Rev. Lett. 54 (1985) 1237.
- [MIW11] K. Miwa et al. , J-PARC E40 experiment.
- [MIY13] T. Miyatsu, M.-Ki Cheoun, and K. Saito, Phys. Rev. C 88, 015802 (2013);
- [MOT10] T.Motoba, K.Itonaga and Y.Yamamoto, Prog. Theo. Phys. Supp. 185 (2010) 197.
- [MOT21] T. Motoba, Special talk at the JPS Meeting, March 12, 2021.
- [MOT88] T. Motoba, H. Bandō, R. Wünsch and J. Zofka, Phys. Rev. C 38 1322 (1988).
- [NAG14][NAG19] MM.Nagels, Th.A.Rijen, Y.Yamamoto, Phys. Rev. C 99 (2019) 044002. (arXiv 1408.4825)
- [NAG15] [NAG19-2] MM.Nagels, Th.A.Rijen, Y.Yamamoto, Phys. Rev. C 99 (2019) 044003. (arXiv 1501.06636)
- [NAG18] S.Nagao, International workshop on the project for the extended hadron experimental facility of J-PARC, March 27, 2018.
- [NAK13] S.N.Nakamura et al., Phys. Rev. Lett., 110 (2013) 012502.
- [NAV00] P. Nvratil, J.P.Vary and B.R. Barrett, Phys. Rev. C 62 (2000) 054311.
- [NOG19] A.Nogga AIP Onc. Proc. 2130, 030004 (2019).
- [NOU19] H.Noumi, High-intensity, high-resolution beam line, Write-ups for workshop on the project for the extended hadron experimental facility of J-PARC (2019), ArXiv:2906.02357.
- [PAN21] P.T.H.Pang et al., ArXiv:2105.08688.
- [PED15]F. Pederiva, F. Catalano, D. Lonardoni, A. Lovato and S. Gandolfi, ArXiv:1506.04042.
- [PET16] S. Petschauer et al., Phys. Rev. C 93 (2016) 014001.

- [PIE08] S. C. Pieper, AIP Conf. Proc. 1011, 143 (2008); Nuovo Cimento Rivista Serie 31, 709 (2008).
- [PIL91] P.H.Pile et al., Phys. Rev. Lett. 66 (1991) 2585.
- [POL06] H.Polinder, J. Haidenbauer, Ulf-G. Meißner, Nucl. Phys. A 779 (2006) 244.
- [PUD95] B. S. Pudliner, V. R. Pandharipande, J. Carlson, R. B. Wiringa, Phys. Rev. Lett. 74, 4396 (1995).
- [RAA21] G.Raaijmakers et al., ArXiv: 2105.06981.
- [REU94] A.Reuber, K.Holinde and J.Speth, Nucl. Phys. A 570 (1994) 543.
- [RIJ10] Th. A. Rijken, M. M. Nagels, and Y. Yamamoto, Prog. Theor. Phys. Suppl. 185, 14 (2010).
- [RIJ99] Th. A. Rijken, V.G.J. Stokes and Y. Yamamoto, Phys. Rev. C 59 (1999) 21.
- [SAN60] J.R. Sanford and C.L. Wang BNL 11279 11679 (1967); C.L. Wang, Phys. Rev. Lett. 25 (1970) 1068.
- [SJO60] B.O. Sjögren., Nucl. Inst. and Meth. 7 (1960) 76.
- [TAK12] T. Takahashi et al., Prog. Theor. Exp. Phys. 2012, 02B010.
- [TAN14] L.Tang et al. (HKS collaboration), Phys. Rev. C 90, 034320 (2014).
- [THI80] H. Thiessem et al., BNL-AGS Proposal E758 (1980).
- [THO99] S. E. Thorsett and D. Chakrabarty, Astrophys. J. 512, 288 (1999).
- [TOY15] T.O.Yamamoto et al., Phys, Rev. Lett. 115 (2015) 222501.
- [TSU98] K. Tsushima, K. Saito, J. Haidenbauer, A.W. Thomas, Nucl. Phys. A 630 (1998) 691.
- [USM95] A. A. Usmani, S. C. Pieper, and Q. N. Usmani, Phys. Rev. C 51, 2347 (1995); A. A. Usmani, Phys. Rev. C 52, 1773 (1995); Q. N. Usmani and A. R. Bodmer, Phys. Rev. C 60, 055215 (1999); A. A. Usmani and F. C. Khanna, J. Phys. G 35, 025105 (2008).
- [WEI12] S. Weissenborn, D. Chatterjee, and J. Schaffner-Bielich, Phys. Rev. C 85, 065802 (2012);
- [WIR18] R. Wirth et al., Phys. Rev. C 97 (2018) 064315.
- [WIR95] R. B. Wiringa, V. G. J. Stoks, and R. Schiavilla, Phys. Rev. C 51, 38 (1995); R. B. Wiringa and S. C. Pieper, Phys. Rev. Lett. 89, 18 (2002).
- [YAM14] Y. Yamamoto, T. Furumoto, N. Yasutake and Th.A. Rijken, Phys. Rev. C 90 (2014) 045805.
- [YAM84] T. Yamazaki, Proc. KEK Int. Workshop on Nuclear Physics in the GeV region, KEK Report 84-20 (1984) 3.